Dissolution Kinetics of Andesitic-Dactic Ash: Experimental Weathering Rate Determinations

Honors Research Thesis

Presented in Partial Fulfillment of the Requirements for the Bachelor of Science Degree, with Honors Research Distinction in Geological Sciences in the undergraduate colleges of The Ohio State University

By

Andrea M. Portier

The Ohio State University

June 2012

Project Advisor: Dr. Anne E. Carey, School of Earth Sciences

Table of Contents

Abstract

Dissolution rates and stoichiometry of the dissolution of basaltic andesites to trachydacitic ash from five volcanic eruptions (1980 Mount St. Helens, USA; 1991 Mt. Pinatubo, Philippines; 2010 Eyjafjallajökull, Iceland; 2010 Pacaya, Guatemala; 2010 Tungurahua, Ecuador) were investigated as part of a study to determine the impact of ash weathering on the potential drawdown of atmospheric CO_2. All ash samples except for the Pinatubo ash were collected within days of deposition. Pinatubo ash was collected in 2008 from the side of a valley that had experienced rapid physical erosion. Ash dissolution experiments were conducted in batch reactors with water or dilute hydrochloric acid over a range of pH (pH ~ 3, 4, 5 and 7) for approximately six months. Dissolution rates and concentrations of major elements and ions (H_4SiO_4, $PO4^{3-}$, Ca^{2+}, Mg^{2+}) were determined from the evolution of solution composition over time. Here after, major elements and ions are referred as Si, PO_4, Ca, and Mg. Ash samples were characterized before and after the experiments by BET surface area analysis, scanning electron microscopy and X-ray fluorescence to determine changes in physical, chemical and mineralogical properties of the ash.

Dissolution kinetics are dependent on the composition, mineralogy, texture, particle size of the ash, and solution pH. Reaction rates increased with increasing acidity, although the pH-dependence of the ash dissolution is complex. Silica concentrations increase approximately linearly over time, and total Si in the experiments increases ~ 2 to 5-fold with increasing acidity. Phosphate concentrations are more variable in solution in comparison to dissolved silica. All experiments showed an initial rapid release of phosphate, and then concentrations either increased more slowly, remained constant, or decreased slightly over time depending on the experiment. The dissolution of trace minerals, such as apatite which is commonly found in igneous materials, may be important because they release nutrients such as phosphate into solution, suggesting an influence in the short-term carbon consumption as biomass. Equilibrium solubility calculations show that solutions are greatly undersaturated with respect to silicate minerals and apatite. The presence of dissolved iron suggests that the solubility of secondary phosphate minerals, such as iron-phosphate present in solubility calculations, may be limiting phosphate release. The solubility and reactivity are key components in determining the volcanic ashes' potential for short-term and long-term CO_2 sequestration.

Acknowledgements

I would like to thank Dr. Berry Lyons, Dr. Ellyn McFadden, Dr. Steve Goldsmith, Dr. Ian Howat, Dr. Carla Restrepo, Alma Quilo, Jeff La Frenierre, and Dr. Bryan Mark for collecting ash samples and help when needed. I would like to thank Dr. Julie Sheets and Brandon McAdams for their technical and analytical help in running analysis of my samples. Furthermore, I would like to thank the Arts & Sciences Research Scholarship and Shell Exploration and Production Company for providing funds to conduct research. I would especially like to thank Dr. Sue Welch and Dr. Anne Carey for their tremendous guidance and support, whom taught and helped me with analysis and interpretation throughout the entire time. Without these people and funds, this thesis would not be possible.

List of Figures

List of Tables

Introduction

The weathering of Ca-Mg silicate rocks and subsequent precipitation of Ca-Mg carbonates in the ocean is a fundamental process in controlling the CO_2 concentration in the atmosphere over geological time (Walker et al., 1981; Berner et al., 1983; Berner, 1999). Research on the erosion of volcanic terrains on high standing islands (HSIs) shows that although the area of these islands only account for only a few percent of Earth's total land surface area, they account for ~30% of the fluxes to the world's oceans (Lyons et al., 2002). Most previous work on the volcanic rocks has focused on the weathering of basaltic terrains (45-52% SiO_2), but recent work has shown that weathering rates of andesitic-dacitic terrains (intermediate rocks with 52-63% SiO_2) on oceanic islands such as the Philippines and other tectonically active areas such as subduction zones are comparable (Goldsmith et al., 2010). This suggests that the weathering of intermediate composition volcanic rocks is more important in controlling atmospheric CO_2 than previously thought. Furthermore, laboratory investigations show weathering of trace Ca-bearing phases in these volcanic rocks, such as apatite, may be important in the total Ca weathering flux for long-term atmospheric CO_2 removal and total P flux for the short-term atmospheric CO_2 removal as biomass. Volcanic rock weathering has been studied by many researchers, but few have studied recently deposited, unconsolidated volcanic ashes.

The overall goal of this research is to understand the importance of andesitic volcanic ash weathering in atmospheric carbon dioxide removal and its subsequent sequestration as Ca- or Mg-carbonate rocks in the marine environment. The specific hypothesis tested for this research is that recent volcanic ashes weather quickly in acidic solutions. Unconsolidated ashes weather more quickly than consolidated volcanic rock. Nutrient release from volcanic ash weathering enhances the overall rate of carbon dioxide removal from the atmosphere through short-term biological removal as plant growth.

2. Geochemical Background

2.1 Silicate weathering and its role in CO_2 consumption

Atmospheric models indicate the relationship between global climate and atmospheric CO_2 content: increased CO_2 leads to warmer temperatures, higher precipitation, and an increase in runoff (Labat et al., 2004; Gislason et al., 2009). The Keeling curve shows that CO_2 concentrations have increased ~25 percent in the last fifty years, from ~310 ppm to 395 ppm due to anthroprogenic activity, primarily the burning of fossil fuels and changes in land use, and concentrations are still on the rise (2012 Scripps CO_2 Program). The annual fluctuation correlates with the CO_2 seasonal signal from the growth and decay of plants and leaves. However, over geological time scales, the weathering of silicate rocks and subsequent precipitation of Ca-Mg carbonates and the burial of organic carbon are the main mechanisms that regulate CO_2 concentrations into the atmosphere (Walker et al., 1981; Berner et al., 1983; Berner, 1999). Silicate rock weathering not only regulates CO_2 concentrations, but also influences the chemistry of the oceans by providing large fluxes of sediments to marine environments (Navarre-Sitchler and Brantley, 2007; Lyons et al., 2005).

The weathering of Ca-rich feldspar, a common silicate mineral, leads to calcium carbonate precipitation according to the following reactions:

$$\underset{\text{Plagioclase}}{CaAl_2Si_2O_8} + 2CO_2 + 3H_2O \rightarrow \underset{\text{Kaolinite}}{Al_2Si_2O_5(OH)_4} + Ca^{2+} + 2HCO_3^-$$

$$Ca^{2+} + 2HCO_3^- \rightarrow \underset{\text{Calcite}}{CaCO_3} + CO_2 + H_2O$$

These reactions lead to a net loss of one mole of CO_2 per mole of feldspar weathered. Similarly, the overall reaction for the weathering of a pyroxene to make carbonate is given by:

$$\underset{\text{Pyroxene}}{CaSiO_3} + CO_2 + 2H_2O \rightarrow CaCO_3 + H_4SiO_4$$

These reactions are controlled by chemical and mechanical weathering of silicates on land coupled to riverine transport of suspended matter, aqueous Ca^{2+} and HCO_3^- to the oceans to react and form calcite and aragonite (Aller, 1998; Gislason and Oelkers, 2003; Gislason et al., 2009). Among the factors affecting weathering rates are temperature, rainfall, erosion rate, lithology (Schopka et al., 2011). Therefore, understanding controls of global weathering rates of silicates is essential to the quantification of the global geochemical cycle of carbon (Lasaga et al., 1994).

Previous work on the weathering of silicate rocks has concluded that basalts yield the highest weathering rates (Meybeck, 1987; Louvat and Allegre, 1997; Dessert et. al., 2003; Rad et al., 2006). Gaillardet et al. (1999) estimated 11.7 x 10^{12} moles of CO_2 are consumed annually by global continental silicate weathering that is strongly associated with high chemical and physical erosion rates (Gaillardet et al., 1999; Lyons et al., 2005; Schopka et al., 2011). Although basalts compose only a few percent of continental rocks, 30-35% of the CO_2 consumption (4.08 x 10^{12} mol/yr) is attributed to basalt weathering (Dessert et al., 2003; Navarre-Sitchler and Brantley, 2007). While most previous work has focused on the weathering of basaltic terrains, recent work has shown that weathering rates of andesitic-dacitic terrains are comparable (Goldsmith et al., 2010) to that of basalt. Andesitic terrains cover a significant portion of total land surface with estimates ranging from 2.4% to 3% compared to estimates of 4.15% to 6% for basaltic terrains (Meybeck, 1987; Amiotte-Suchet et al., 2003; Goldsmith et al., 2010). Andesitic terrains are often associated with tectonically active margins, such as subduction zones, where high physical and chemical erosion rates generally occur, compared to that of basaltic terrains which occur generally outside these climatic zones (i.e. Columbia River, Siberia Traps) (Goldsmith et al., 2010).

In addition to tectonically active areas such as subduction zones of andesitic material, research on weathering of volcanic terrains on high standing oceanic islands (HSIs) shows that although these areas account for only a few percent of the land surface area, they account for much of the modern weathering flux to the world's oceans (Lyons et al., 2005). These regions have abundant ultramafic to intermediate volcanic rocks, are tectonically active, have high erosion rates, and experience warm and wet climate (Schopka et al., 2011). Weathering on geological provinces, such as HSIs associated with plate boundaries, island arcs, and andesitic mountain chains, may have influenced past atmospheric CO_2 concentrations (Lyons et al., 2005).

Atmospheric CO_2 removal from the weathering of andesitic-dacitic ashes may be equally as important as from the weathering of andesitic-dacitic volcanic rocks in areas that are highly tectonically active and high erosion rates are present such as subduction zones and HSIs. Dissolution of recent volcanic ashes may have potential not only for long-term removal of CO_2 but short-term removal of atmospheric CO_2.

2.2 Limiting role of iron and phosphorous

While silicate weathering is known to regulate the long-term CO_2 cycle, it can also affect short-term CO_2 uptake by releasing trace nutrients that enhance primary productivity on land and in the ocean. Soils formed on volcanic materials are highly fertile due to the abundance of micro- and macro-nutrients of silicate glass and minerals from weathering (Schmincke, 2004; Duggen et al., 2010).Volcanic ash dissolution and transport to the ocean can introduce significant amounts of bio-available iron and phosphorous (Duggen et al., 2010). Iron is a key limiting micro-nutrient for marine primary productivity (Langmann et al., 2010), while phosphorous (P) is a key limiting macro-nutrient for removing carbon as biomass (Jones and Gislason, 2008).

Several studies suggest that volcanic ash deposition has a short-term influence on atmospheric CO_2 concentrations via dissolution of iron (Fe) and phosphorous (P). For example, Duggen et al. (2007) demonstrated that ash-derived iron can boost phytoplankton growth in iron-limited areas of the ocean. Furthermore, Sarmiento (1993) suggested that the relative drawdown of atmospheric CO_2 in the Northern Hemisphere was a result of increased marine primary production fertilization due to Fe-fertilization of the Southern Ocean by Pinatubo ash one to two years after the 1991 eruption. The initial release of phosphorous and iron from volcanic ash is likely to play a role in the short-term drawdown of atmospheric CO_2 from an increase in primary production. However, the limitations of phosphate release through the adsorption of phosphate onto Fe-oxides need to be considered.

2.3 Dissolution of volcanic glasses compared to crystalline counterparts

Dissolution rates for both glasses and minerals are influenced by a number of factors including pH, temperature, chemical composition, and reactive surface area. Previous experimental work has demonstrated that dissolution rates of glassy materials are faster than for corresponding rates for minerals, but only for Si-rich materials (more felsic) (Wolff-Boenisch et al., 2005). On the other hand, Si-poor glasses and minerals (more mafic) exhibit similar dissolution rates to one another. Dissolution rates of basalts weather 10-100 times faster than Si-rich rocks with rates consisting approximately of 9.06×10^{-11} ($mol_{Si}/m^2/s$)(glassy) and ~5.01×10^{-13} ($mol_{Si}/m^2/s$) (crystalline) of Si-poor rocks compared to 1.09×10^{-11} ($mol_{Si}/m^2/s$) (glassy) of Si-rich rocks at ~25º C and pH 4 solutions (Gudbrandsson et al., 2011).

The release of Ca and Mg in basalts is faster than in its Si-rich counterparts. Ca release rates of natural glasses are greater than those of crystalline rocks in felsic to mafic minerals (Wolff-Boenisch et al., 2006). Furthermore, Ca release rates of basalt or gabbro are approximately two orders of magnitude faster than rhyolite or granite (Wolff-Boenisch et al., 2006).

2.4 Geologic Setting

2.4.1 Mount St. Helens

Mount St. Helens (46.20º N, 122.18º W) is an active stratovolcano located in the Cascade Range of Washington, United States. It is composed of layers of basalt and andesite with a dacite dome in the central crater reaching an elevation of 8,363 feet (Brantley and Myers, 2005; Cashman et al, 2005). Past eruptions have a wide compositional range of lavas and pyroclastic deposits (Lockwood and Hazlett, 2010). The May 1980 eruption of Mount St. Helens erupted catastrophically, generating a lateral blast of pyroclastic flow and fall deposits (Farlow et al, 1981) that covered over ~600 km^2 (Cashman et al 2005; Ongaro et al, 2011). A vertical plinian phase following the blast emitted more than 1.08 km^3 of volcanic ash that circled the earth in 15 days and deposited up to 70 mm or more in depth (USGS; Bernstein et al., 1986). The 1980 volcanic ash consists of dacitic ash particles ranging from 63-4000 µm containing glass, plagioclase, hornblende, and pyroxenes (Fero et al. 2008; Farlow et al, 2012). This eruption caused 57 deaths, numerous health effects and damage to wildlife (USGS; Bernstein et al., 1986).

2.4.2 Mt. Pinatubo Volcano

Mt. Pinatubo, located in the Philippines (15.13º N, 120.35º E), is part of a chain of composite volcanoes that belong to the Bataan calcalkaline arc (southern end of the Luzon arc) and reflects eastward subduction of the South China Sea Plate along the Manila Trench (Di Muro et al. 2008). The volcano is a stratovolcano of a composite of hornblende-dacite dome constructed upon older volcanoes, sedimentary strata, lahar and pyroclastic-flow deposits and it is underlain by an ultramafic complex (Pierson et al. 1992: de Hoog et al. 2003).

The paroxysmal eruptions in 1991 of Mt. Pinatubo (June 12th and 15th) from the mixing of magmas produced tephra fall, pyroclastic flows, and surges (de Hoog et al. 2003: Pallister et al. 1992). The June 12th tephra deposits contained hornblende plagioclase scoria with the bulk rock composition composed mainly of andesite. Eruptive products contained minerals of augite, olivine, quartz, and anhydrite, and glass with disequilibrium compositions within the andesitic material (Pallister et al. 1992). The June 15th eruption ejected 7-11 km³ of airfall tephra and pyroclastic flow deposits, and emitted more than 17 Mt of SO_2 and up to 230 Mt of CO_2 into the atmosphere (Newhall et al. 1996). The eruption produced two types of juvenile dacite: white crystal-rich pumice and gray to tan pumice which was crystal poor (Pallister et at. 1992; Newhall et al. 1996). The volcano stood at the height of 1,745 meters before the 1991 eruption, leaving a large 2.5 kilometer-wide collapse caldera with a height (high point of caldera rim) of 1,485 meters after the 1991 eruption (Newhall et al. 1996).

Pinatubo's eruptions of 1991 produced a decrease in temperature by 0.5ºC worldwide due to the SO_2 and CO_2 emissions. The eruption killed about 800 people and more than one million people were displaced (Newhall et al. 1996).

2.4.3 Eyjafjallajökull

Eyjafjallajökull volcano (63.38º N, 19.36º W: 1666 m above sea level) is located in the southern tip of Iceland's Eastern Volcanic Zone, which is the most active part of the Neovolcanic zones there (Dellino et al., 2012). The volcano is an ice-covered stratovolcano with known eruptions dating back to 920 BC (Keiding and Sigmarsson, 2011).

The 2010 eruptions began in March with small flank eruptions, which produced negligible ash. On April 14, an explosive phase eruption began that emitted fine-grained phreatomagmatic ash. Eyjafjallajökull ash is dominated by andesitic glass, plagioclase, pyroxene, and olivine (Gislason et al., 2010). The ash particles ranged from a few tens of nanometers to more than 300 µm in diameter (Gislason et al., 2010). Ash loadings from satellite data found that ash emissions into the atmosphere reached 8 ± 4 Tg (Stohl et al., 2011; Thorsteinsson et al., 2012). This eruption lasted six weeks and created unprecedented disruptions in air traffic during April 15-21 and numerous health problems (Gislason et al., 2011; Carlsen et al., 2012).

2.4.4 Pacaya Volcano

Pacaya volcano (14.38° N, 90.6° W, 2552 m) is an active andesitic stratovolcano located on the southern rim of the Pleistocene Amatitlán caldera in Guatemala (Conway et al., 1992;

Dalton et al., 2010). Pacaya has been active since 1965 with frequent strombolian eruptions with intermittent lava flow extrusion and occasional larger explosive eruptions. The modern cone is composed of lava flows and tephra, and andesitic-dacitic domes (Dalton et al., 2010). Past eruptions have resulted in numerous deaths, infrastructure damages, and closing down Guatemala's international airport for three days (Rodriguez et al., 2004).

The May 2010 eruption ejected tephra 500 m into the air which then drifted downwind 20-30 km resulting in infrastructure damage in Guatemala City and Antigua. Ash continued to be ejected during May- September, 2010 emitting over 8.5 x 10^6 m^3 of tephra into the atmosphere (Gomez et al., 2012; USGS).

2.4.5 Tungurahua Volcano

Tungurahua Volcano (1.467° S, 78.442° W) is one of the most active volcanos in the Eastern Andean Cordillera in Ecuador (De la Cruz-Reyna et al, 2010). The current period of unrest (1999-present) has resulted in numerous medical problems, deaths of animal livestock, and damages to infrastructure (Le Pennec et al 2008; Biggs et al., 2010). It is a steep-sided andesitic stratovolcano with an approximate height of 5020 m (Biggs et al, 2010: De la Cruz-Reyna et al, 2010). Since 1999, eruptions have had uneven intensity phases, from mild strombolian eruptions to vulcanian that produced widespread ash fall and pyroclastic flows with compositions ranging from basaltic andesites to dacites (Hall et al., 1999; Ruiz et al, 2006; Le Pennec et al., 2008; Biggs et al., 2010; Eychenne et al., 2012).

Past research has shown that modern Tungurahua Volcano has maintained a magma production rate of approximately 1.5×10^6 m^3/yr for the last 2300 years (Hall et al., 1999: De la Cruz-Reyna et al, 2010). The 2006 and 2007-2008 eruptions varied immensely in regards to volume of ash and pyroclastic flow deposits. Approximately 42–57$\times10^6$ m^3 was erupted in the August 2006 eruption and 1.7 x 10^6 m^3 was erupted in the 2007-2008 eruption (Biggs et al, 2010; Eychenne et al, 2012). The December 2010 eruption's ash cloud reached 3 km above the volcano's crater causing numerous people to evacuate their homes surrounding the volcano (http://articles.cnn.com/2010-12-04/world/ecuador.volcano_1_volcano-ash-cloud-ash-and-lava?_s=PM:WORLD).

3. Materials and Methods

3.1 Ash sample collection

Five samples were obtained from andesitic-dacitic volcanic terrains varying from eruption date and type, and bulk chemistry (Fig. 1). Ash samples were collected at varying times post eruption, most collected from hours to days after eruption, but the Pinatubo ash sample was collected 17 years post-eruption. Since collection, the volcanic ashes were stored in closed glass vials (Mount St. Helens, Pacaya), or in translucent polypropylene Nalgene™ bottles (Eyjafjallajökull, Tungurahua), or Ziploc® bags (Mt. Pinatubo) at room temperature. Several of the ashes were allowed to air dry after collection, however there was no other substantive pretreatment. The oldest ash sample is from the 1980 eruption of Mount St. Helens (USA) donated by Dr. Berry Lyons and Dr. Ellyn McFadden of Ohio State University. Ash was collected from the 1991 eruption of Mt. Pinatubo (Philippines) on the island of Luzon by Dr. Anne Carey and Dr. Steve Goldsmith of Ohio State University, School of Earth Sciences, during January 2008 at the bottom of Mt. Pinatubo's flank. Recent ash samples of the 2010 eruption of Eyjafjallajökull (Iceland) were collected and donated by Dr. Ian Howat of Ohio State University, School of Earth Sciences, approximately 16 miles east of the eruption site during the April 2010 eruption. Pacaya ash (Guatemala) was collected by Alma Quilo of the Universidad del Valle de Guatemala in Guatemala City, northeast of the Pacaya Volcano, approximately 6-7 hours after the initial May 2010 eruptions. The most recent ash sample is from approximately 5 km southwest from the vulcanian summit of Tungurahua (Ecuador), and was collected from the leaves of bushes during Tungurahua's eruptive period on December 25, 2010. Ash was collected and donated by Jeff La Frenierre and Dr. Bryan Mark, of Ohio State University, Department of Geography.

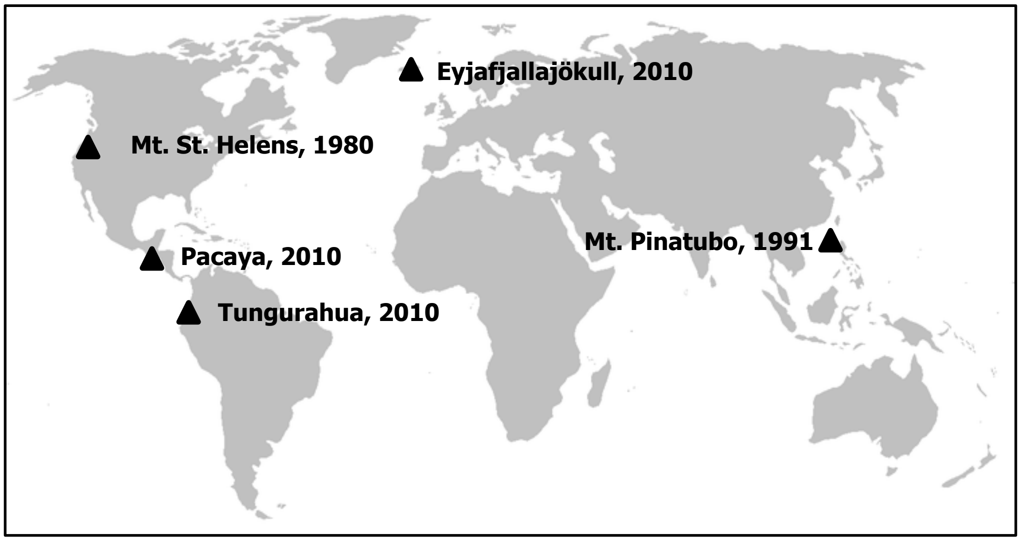

Fig.1. Locations of volcanic ash samples used in dissolution experiments and the year of eruption

3.2 Ash sample characterization

Preliminary characteristics of the ash samples (such as color and particle size) were noted by visual inspection (Table 1). With the exception of the Pinatubo ash, ash samples were unsieved, however ash particles sizes were approximately homogenous in each sample. The Pinatubo ash was sieved with a 2 mm size to remove some of the larger fragments. Bulk chemical analyses of these ash samples were determined using X-ray fluorescence using a PANalytical MagiX Pro PW2440 XRF instrument using methods of Goldsmith et al. (2008). Ash samples were ground using a mortar and pestle and then an aliquot of this material was fused into a borosilicate bead (1:4 sample:flux) for bulk chemical analysis. XRF total errors for sample concentrations did not exceed ±10%. Surface area was determined by nitrogen gas sorption (BET) (Brunauer et al., 1938) using a Micromeretics Instrument. Ash samples were characterized using an FEI Quanta FEG 250 Scanning Electron Microscope equipped with a Brucker EDS detector. Collected ash samples were placed on carbon tape and coated with Au-Pd before analysis. Reacted samples were gently rinsed with MilliQ water, allowed to air dry, then treated similarly. Most samples were imaged at 15 kV accelerating voltage and working distance of 13 mm.

Table 1.
Summary of bulk ash sample compositions from X-ray fluorescence analysis (%)

	Tungurahua	Pacaya	Eyjafjallajökull	Mount Pinatubo	Mount St. Helens
Classification	Andesite	Basaltic Andesite	Trachy-andesite	Trachydacite	Trachy-andesite
Eruption Style	Explosive	Strombolian	Explosive	Explosive	Plinian
Type of Ash	Fine	Coarse	Fine	Coarse	Fine
Eruption date	December, 2010	May 27, 2010	April, 2010	June 12-15, 1991	May 18, 1980
Collection date	December 25, 2010	May 27, 2010	April, 2010	January, 2008	Unknown
Sample Site	5 km SW	Guatemala City (30 km NE)	25.8 km E	Bottom of flank	Unknown
SiO_2	59.91	51.59	54.88	62.24	57.07
TiO_2	0.85	1.20	1.52	0.51	1.10
Al_2O_3	16.43	17.61	13.75	14.53	15.65
Fe_2O_3	10.97	11.10	9.72	4.47	6.65
MnO	0.11	0.18	0.22	0.11	0.10
MgO	4.43	4.97	2.34	2.35	2.60
CaO	6.73	8.79	5.02	4.59	5.93
Na_2O	3.83	3.39	9.50	7.86	8.27
K_2O	1.71	0.87	1.82	1.67	1.21
P_2O_5	0.23	0.26	0.36	0.19	0.23
Loss On Ignition	0.12	0.33	0.88	1.48	1.20
Total	101.32	99.96	99.12	98.52	98.80

Eruption type and collection information is shown. Sample concentrations had precisions of ≤0.2 and accuracy of ±2%.

3.3 Experimental methods

Ash dissolution experiments were conducted in 500 ml amber polypropylene Nalgene™ bottles. Bottles were rinsed several times with MilliQ water, soaked for several hours in MilliQ, and then rinsed again before use. At the beginning of the experiment, MilliQ water (500 mL) was added to each of the forty polypropylene bottles used (eight bottles for each ash, two bottles for each pH) for this experiment. Aliquots of 1N HCl was added to create solutions with initial pH of ~3, 4, 5, and 7 (deionized MilliQ water was assumed to be pH 7). 1 g of ash was weighed and added to the prepared solutions of pH 3, 4, 5, and 7 and stored at 22°C.

Solution aliquots were removed from experimental solutions using a sterile 20 ml Norm-Ject® syringe and filtered through a 45µm pore size 25mm diameter nylon GD/X disposable filter directly into new sterile Falcon Max™ Jr. 15 ml polystyrene conical tubes and Ion Chromatograph(IC) autosampler vials for cation and anion analyses prior to use. IC autosampler vials were rinsed with deionized water (18MΩ) and soaked for 24 hours, then rinsed three times with deionized water (18MΩ) before placing tubes in a laminar flow hood to dry prior to use. Filter blanks were created by filtering deionized water into vials using the same methods used for samples. Samples were stored in a refrigerator at 4º C until analysis. A separate solution aliquot was collected for pH analysis. Solution pH was measured with a gel filled electrode and a Thermo-Orion pH meter 420a that had been calibrated with standard buffers. A total of 412 aliquots were collected for the dissolution experiments.

Concentrations of major cations (Ca^{2+}, Mg^{2+}, K^{+}, Na^{+}, Li^{+}) and anions (SO_4^{2-}, PO_4^{3-}, Cl^{-}, F^{-}) were determined from ion chromatography (IC), with a Dionex DX-120® ion chromatograph using the methods of Welch et al. (1996). Precision was determined using five replicate check standards per run with relative standard deviations of ±1% and no greater than ±5%. Dissolved concentrations of silicate and phosphate were measured using a Skalar Sans++ nutrient analyzer with determination of precision by using 15 standards with a drift and a wash run every ten samples. Replicate analyses had precisions usually less than ±5%.

Total and reduced iron analyses were conducted on selected samples using a modified ferrozine method (Stookey, 1970; Santelli et al, 2001). Samples were not initially analyzed because facilities were not available. However, an additional peak was observed in the cation chromatograms, indicating that Fe release was important in the overall dissolution reaction. A separate set of experiments was conducted at pH 4 to estimate iron release from the volcanic ash. These experiments were set up similarly, except they were scaled down to solution to a solid ratio of 100ml: 0.2g. These experiments were sampled after 11 days. Iron was measured on selected samples from the first set of experiments approximately 14 months after the start of these experiments. Total and reduced iron were measured on all the separate batch experiments and selected batch samples.

Geochemical modeling using PHREEQC was conducted with measured major solute concentrations in order to determine speciation and saturation state indices for expected primary and secondary mineral phases present in batch sample solution using methods of Parkhurst and Appelo (1999). Conditions at 2 and 23 weeks (sampling time 3 and 10) were chosen for modeling. Since dissolved iron had not been measured, iron concentrations were estimated for a maximum concentration from the peak area in the chromatogram program after the third sampling event using estimated concentrations of 10^{-3} and 10^{-4} ppm of Fe^{2+} and Fe^{3+}. Furthermore, ferrous and ferric concentrations for sampling event 10 were estimated from the selected samples used from the ferrozine method that were conducted ~14 months after initial time of experiments.

4. Results

4.1 Ash geochemistry

The ash samples range from basaltic andesite to trachydacite (Fig. 2, Table 1). Bulk chemical compositions of these ash samples show relatively high Si levels and moderate levels of Ca and Mg for Tungurahua, Mt. Pinatubo, and Mount St. Helens (Table 1). Comparatively, Eyjafjallajökull and Pacaya have low Si levels and intermediate to high levels of Fe, P, Ca and Mg (Fig. 2, Table 1). Particle size distribution varies from homogenous and fine grained ash (Mt. St. Helens, Eyjafjallajökull, Tungurahua) to coarser and more heterogeneous (Mt. Pinatubo, Pacaya). The particle surface area per gram from experimentally measured BET specific surface area (A_{BET}) analysis ranged from 0.143 m^2/g to 6.15m^2/g (Table 2).

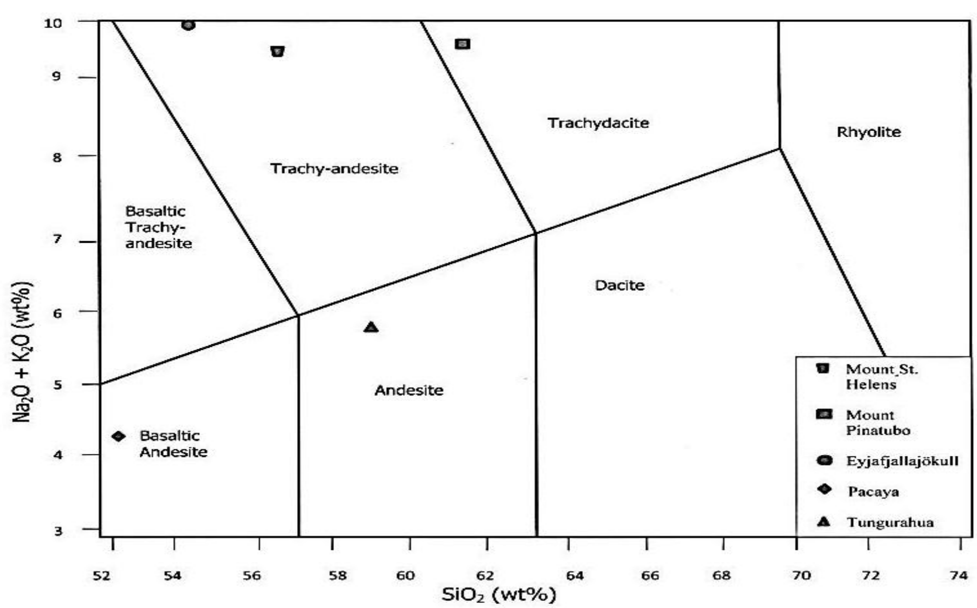

Fig. 2 Classification of samples based on volcanic ash silica content and alkali metal concentrations (Le Bas et al., 1986). Sample compositions range from Basaltic-Andesite to low Si Dacite.

Ash Sample	Mount St. Helens	Pinatubo	Eyjafjallajökull	Pacaya	Tungurahua
Specific Surface Area (A_{BET}) (m^2/g)	0.783	0.698	6.15	0.143	0.247

Table 2. Specific surface area (A_{BET}) of volcanic ashes before dissolution experiments

Figures 3-7 show Scanning Electron Microscope (SEM) images of the five ash samples before and after dissolution experiments. The composition, mineralogy and morphology of the samples varied considerably among ash samples. The SEM images and EDX analysis show glassy felsic matrixes containing phenocrysts of feldspars, pyroxenes, amphiboles, olivines, and phosphates along with iron-titanium rich euhedral crystals (often hexagonal in shape). The Pacaya and Pinatubo samples are moderate-highly vesicular, consisting of smaller glass fragments, euhedral Fe-Ti rich crystals, and various anhedral to euhedral grains composed mainly of Mg, Ca, Si that are smaller than 10µm (Figs. 3 & 4). Pre-dissolution phase of both of these ashes display an abundance of glassy fragments and iron-rich crystals on the surface with aggregates of these grains located in vesicles. SEM images of Pinatubo ash shows evidence of large apatite crystals; Pacaya displays evidence of detached or dissolved euhedral crystals from host particle's matrix. Mount St. Helens, Eyjafjallajökull, and Tungurahua ashes (Figs. 5, 6, & 7) display a low-moderate vesicular texture with evidence of anhedral to euhedral Fe-rich and Ca, Mg, K-silicate minerals set in a fine grained to glassy matrix. Surface coatings and fragments are glassy to Fe-Mg rich and potential iron non-silicates in composition with particles less than 10µm. Mount St. Helens shows detachment and/or dissolution of apatite and pyroxenes.

Comparative to their fresh counterparts, post-experimental ashes had evidence of site specific reactions and evidence of undissolved phases of glass. They demonstrate varying sizes of dissolution pits, dissolution features such as dissolved surface areas (Pacaya), dissolution of phenocrysts, and show evidence of possible precipitates. Post-experimental SEM images show fine grains of crystalline (mainly Fe-rich), amorphous, and glassy material still attached to host particle matrix and/or surface and dissolution of euhedral apatite and hexagonal structure crystals (especially Mount St. Helens, Mt. Pinatubo). Post-experimental SEM images contain clear evidence of the very crystalline ash material of Tungurahua and Pacaya. These ashes display intact crystalline material with dissolution of amorphous glass surrounding adjacently to the phenocrysts along with detachment or dissolution of pyroxenes, amphiboles, or olivines from host grain. The Tungurahua images show rough and smooth surfaces that contain bubbles creating more porosity within the grains of ashes (Fig. 7). Pinatubo ash displays clay-like particle textures on the surface edge of vesicles and large dissolved euhedral crystals greater than 3µm in diameter (Fig. 4). Furthermore, Pinatubo ash displays areas that are calcium rich that may be attributed to the presence of attached gypsum or other sulfides and salts on depleted solid phase. This could explain moderate loss on ignition observed when calculating bulk chemical analyses (Table 1). Although Eyjafjallajökull ash shows undissolved phases of crystals, predominantly that are euhedral in shape and large in size, the ash displays many areas that contain dissolution pits up to 20µm (Fig. 6). Mount St. Helens shows dissolved hexagonal crystals with an atomic composition close to apatite and undissolved euhedral crystals throughout grains consisting of Fe-Ti as well as non-iron silicates and Ca-Mg-silicates (Fig. 5). SEM analysis (before and post-experimental) is fairly consistent with the observed XRF bulk chemistry, where bulk chemical data is represented in SEM images, especially the presence of Fe-Ti rich minerals that directly correlate with high levels of iron and titanium in XRF data, and various traces of the mineral apatite from Mount St. Helens, Pinatubo, and Eyjafjallajökull ash that would explain moderate levels of P in sample.

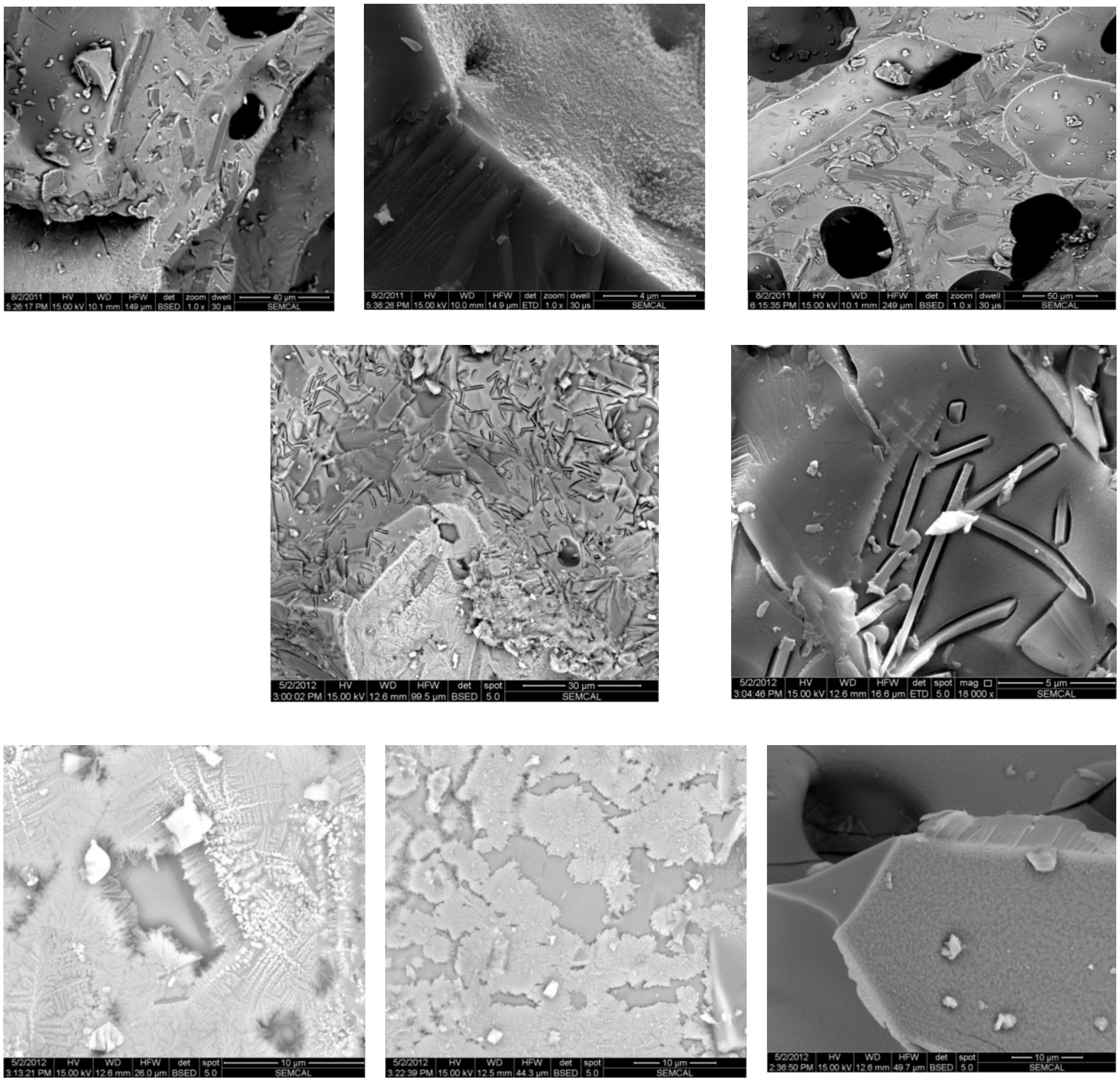

Fig. 3. SEM images of Pacaya ash. Top three images show ash before experiments. Bottom five are SEM images of ash post-experimental, samples were taken from batch experiment bottles. Note dissolved crystal phases and dissolved glassy phases in second row.

Fig. 4. SEM images of Pinatubo ash. (Right) Ash images before experiments. (Below) Ash images post - experimental, samples were taken from batch experiment bottles. Note the presence of Fe-rich crystals (lighter color minerals). Euhedral hexagonal dissolved crystals of apatite present in row 3.

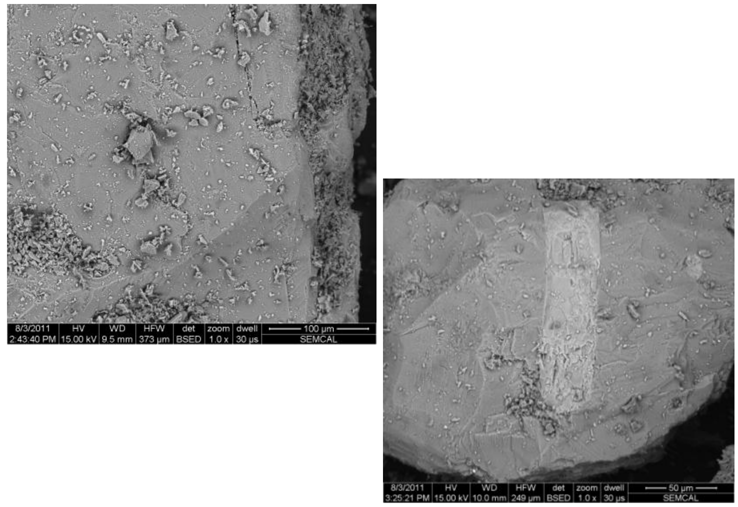

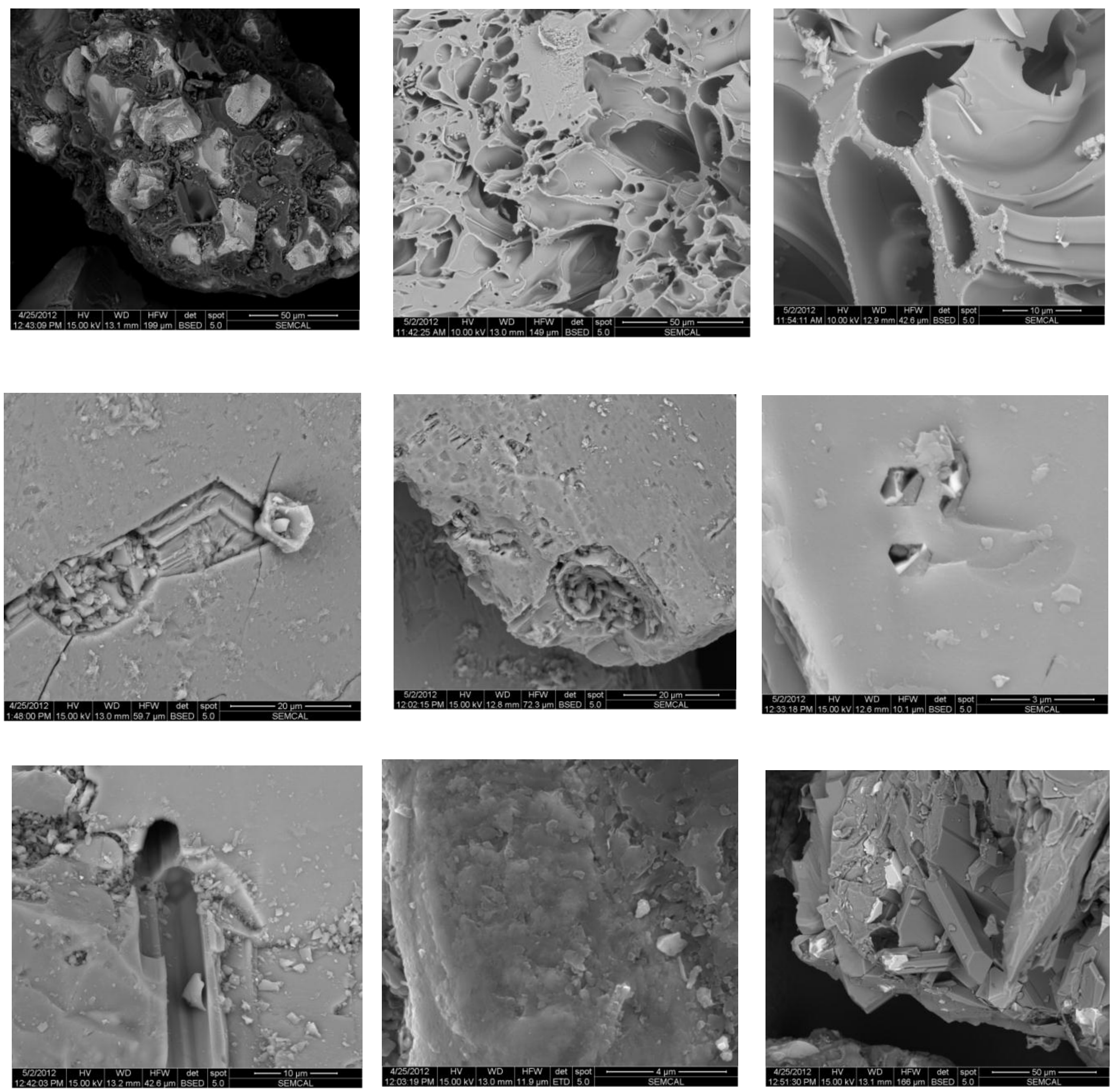

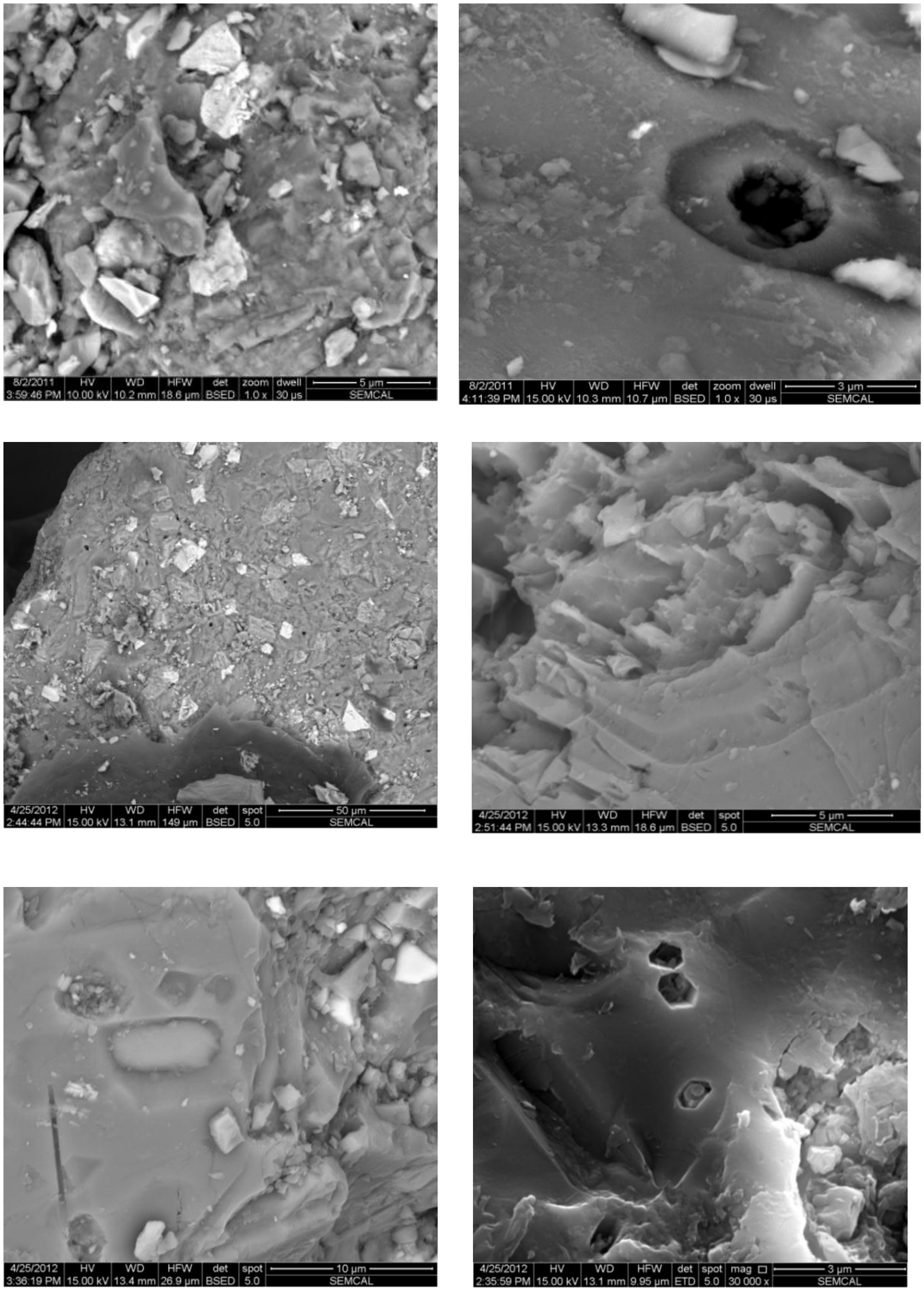

Fig. 5. SEM images of Mount St. Helens ash. Top row shows ash before experiments. Bottom four display ash post-experimental, samples taken from batch experiment bottles. Note dissolved hexagonal crystals of apatite.

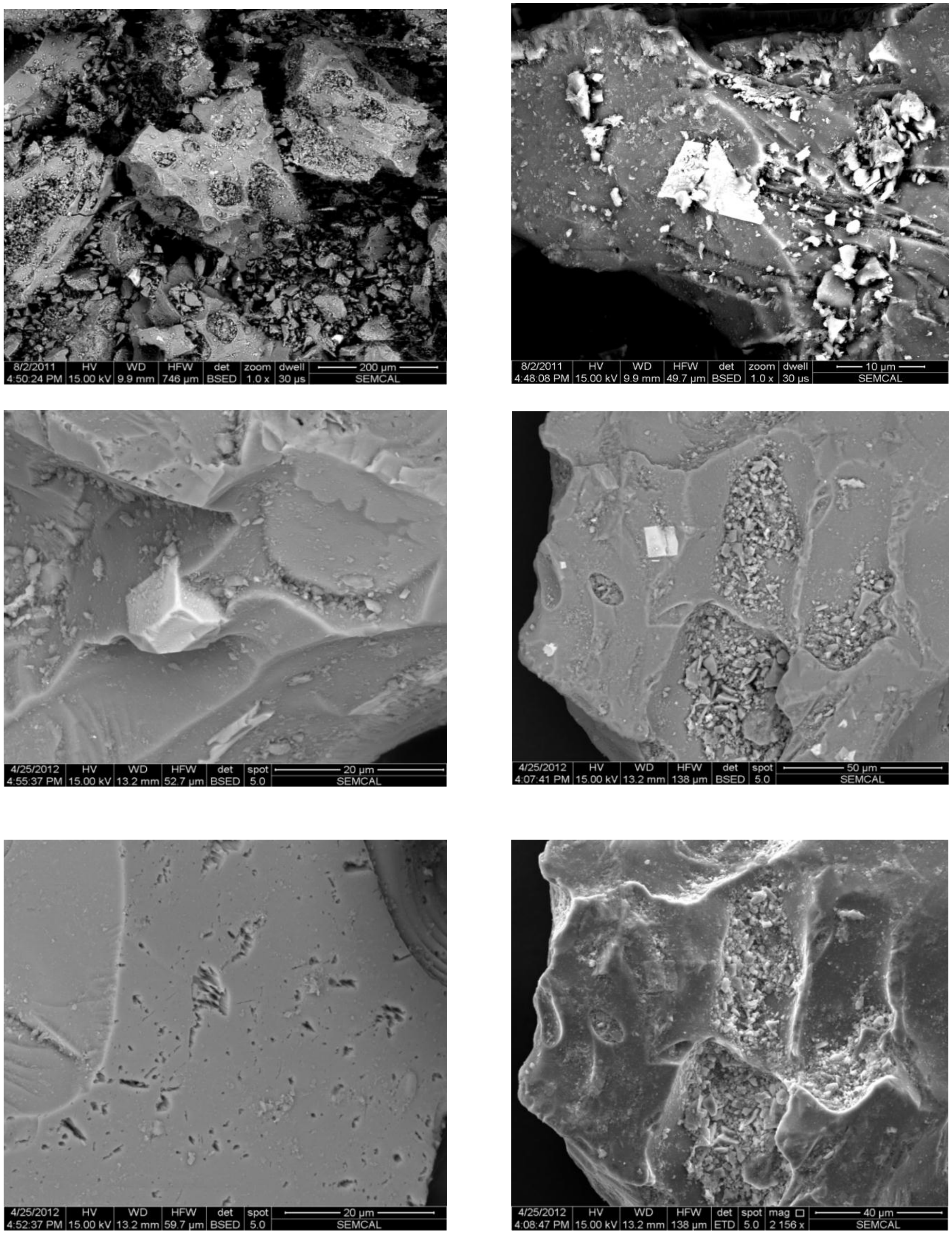

Fig. 6. SEM images of Eyjafjallajökull ash. Top two images show ashes before experiments. Bottom four show ashes post- experimental, ash extracted from batch experiments. Note dissolution pits and partially dissolved Fe-rich crystals.

Fig. 7.SEM images of Tungurahua ash.
(Right) Image before experiments.
(Below) Images post-experimental of the ashes, taken from batch experiments. Note euhedral Fe-Ti rich crystals and dissolved phenocrysts and glassy phases.

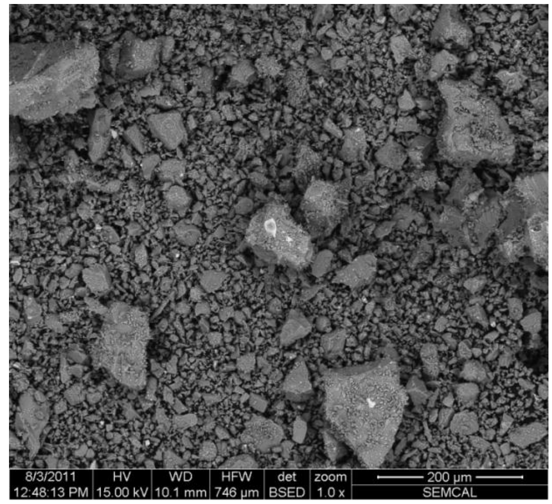

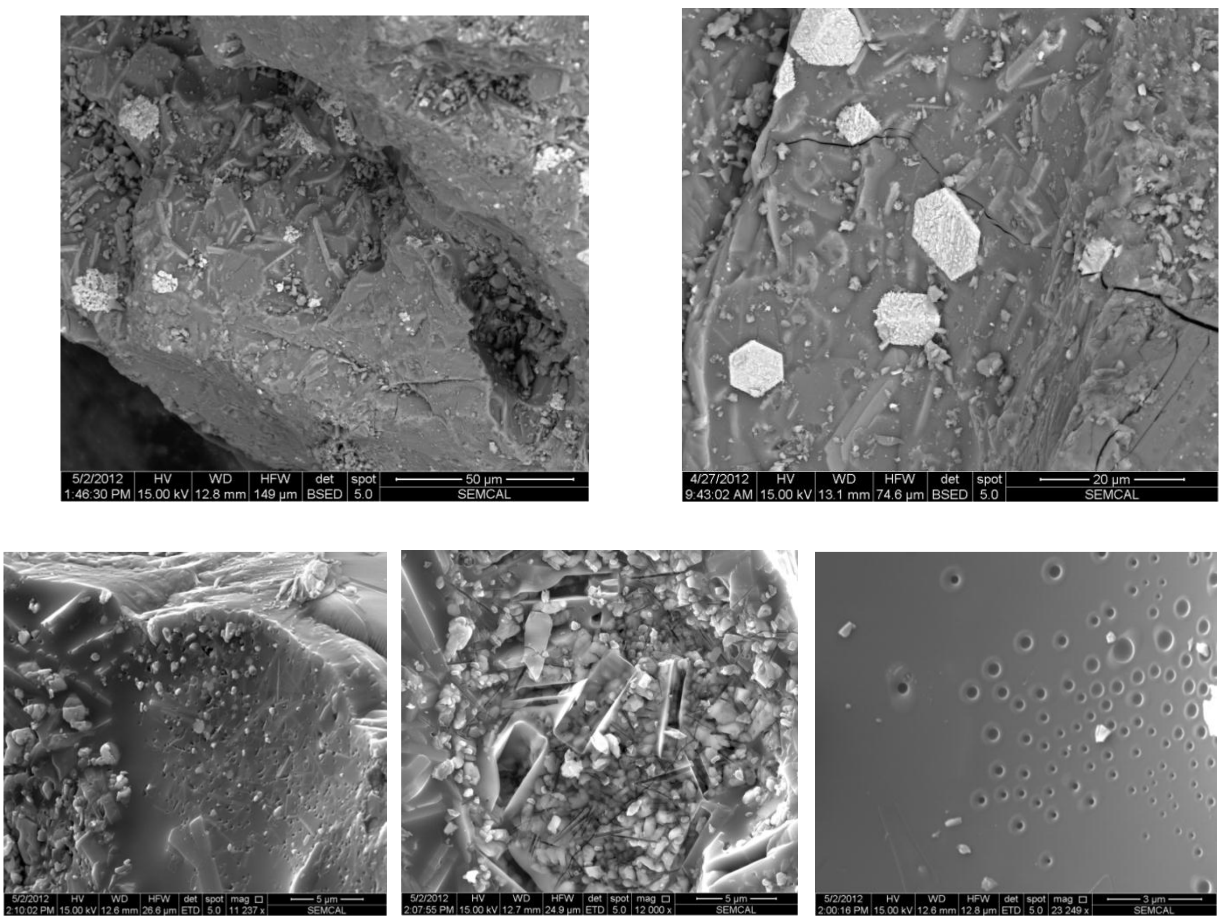

4.2 Experimental results of ash dissolution

The concentrations of major elements measured in solution from the batch experiments are summarized in Appendix A, respectively. Each ash was reacted in acidic to neutral solutions at initial pH 3, 4, 5, and 7. The results of all the experiments were different depending on pH and ash composition, but there were some general trends observed. The pH in all the acidic experiments increased over time, indicating an acid-consuming dissolution reaction. The concentrations of solutes from the reacting ash increased over time, corresponding to the change in pH. The pH varied considerably in the water-leach experiments, some increasing, some decreasing.

4.2.1 Si release

Silicate concentration in solution will be used as an overall indicator of reaction progress. In all the dissolution experiments, Si concentrations increase approximately linearly over time (Fig. 8). For each ash, the Si in solution increases ~2 to 5-fold with increasing acidity. Eyjafjallajökull had the highest release of Si compared to all other ashes with up to ≥390µM over the duration of the experiment followed by Pacaya's Si release of ~330µM over the eight months. High Si release from these ashes is consistent with SEM images of post-experimental solid phase which show relatively small amount of glassy surface fragments still attached to host grain and glassy dissolution around phenocrysts. Furthermore these ashes had the fastest initial Si release (up to ~70µM) within the first 48 hours. In comparison, Mount St. Helens, Pinatubo, and Tungurahua had slightly lower Si releases of ≤250µM (initial up to 30µM), which Si could be attributed to the slower dissolution of minerals rather than Si release from glassy materials (initial and over time) seen with Eyjafjallajökull and Pacaya.

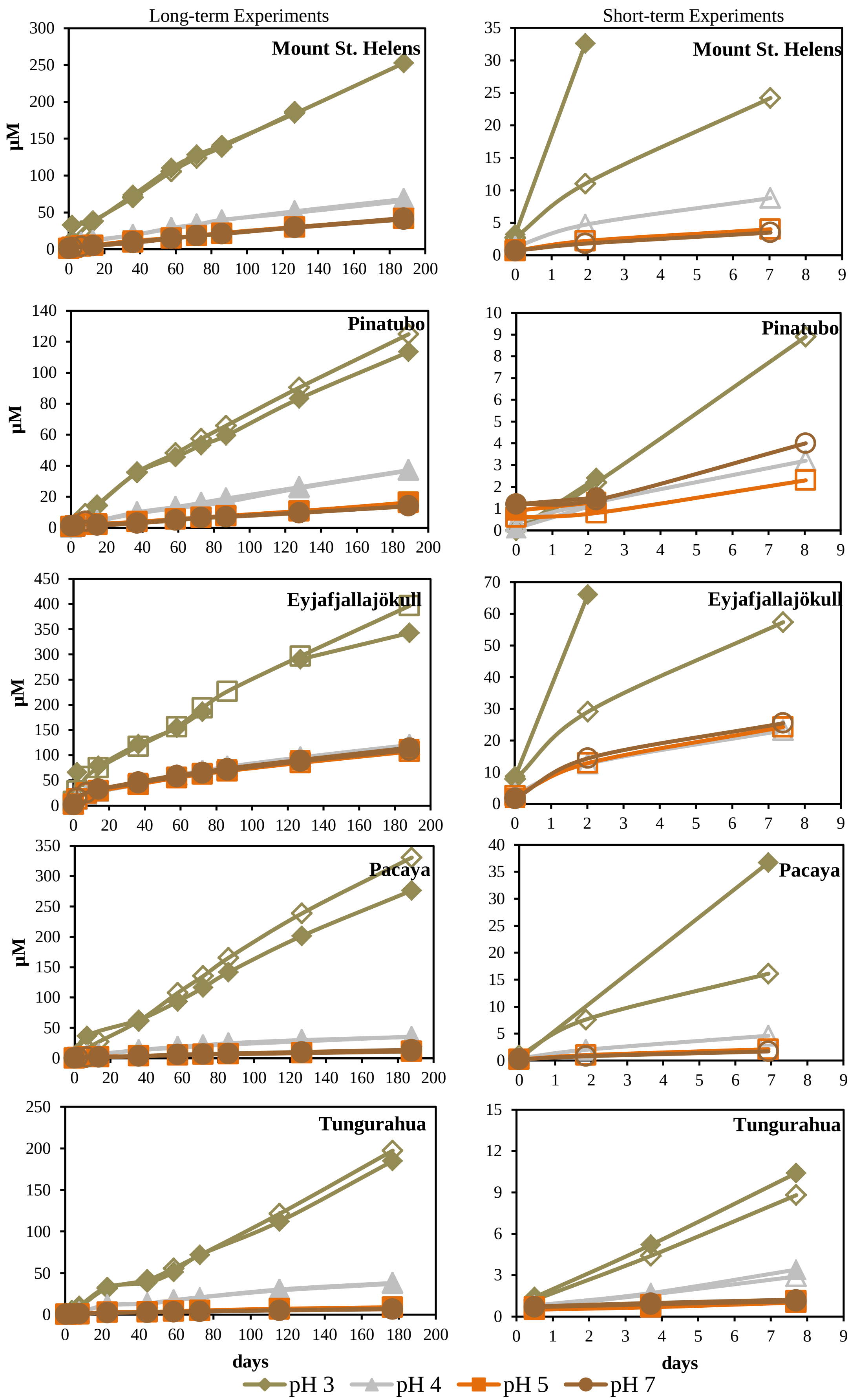

Fig. 8. Si concentrations over time of volcanic ashes in solution ~pH 3, 4, 5, 7 with replicate experiments. Note different vertical scales for each ash.

4.2.2 Ca-Mg release and other major ions

Release of other ions, especially divalent cations (Ca, Mg) was variable with initial rapid releases into solution over hours to days. Ca and Mg initial rapid release from all ashes occurred within the first 48 hours of the experiments followed by a slower increase in concentration of major cations, or concentrations that remained approximately constant over the rest of the experimental time period. Eyjafjallajökull had the highest initial release of Ca, ~150µM, followed by Pinatubo with ~140µM Ca. In other ashes, initial Ca concentrations were 80µM or lower. Mg concentrations were relatively high in pH 3 solutions compared to concentration in pH 4, 5, and 7 solutions. Mount St. Helens, Eyjafjallajökull and Pinatubo released the lowest amount of Ca and Mg compared to their bulk chemistry from XRF analysis. This suggests that the Ca and Mg concentrations are originating from resistant Ca-Mg silicates and not from apatite. Furthermore, the initial rapid increase represents the possible dissolution of adsorbed surface metal salts and other surface fragments that contain the major cations as well as Fe, SO_4^{2-}, and F^- that react and dissolve with these divalent cations. See Appendix A, Fig. 1A-5A for graphs of major ions versus time.

Relative to all ions measured, the highest concentrations of ions at the end of the experiments (time sampling point 10) , primarily Si (≤ 396 µM, Ca (≤ 242 µM), and F^- (≤ 19.0 µM) are found in Eyjafjallajökull pH 3 samples, followed by Pinatubo with high concentrations of Si, Ca, and F^-, along with the highest concentrations of SO_4^{2-} (≤ 81 µM). Mount St. Helens contains the highest concentrations of Mg (≤ 102.6 µM). However, major anions such as F^- may have little influence solution chemistry.

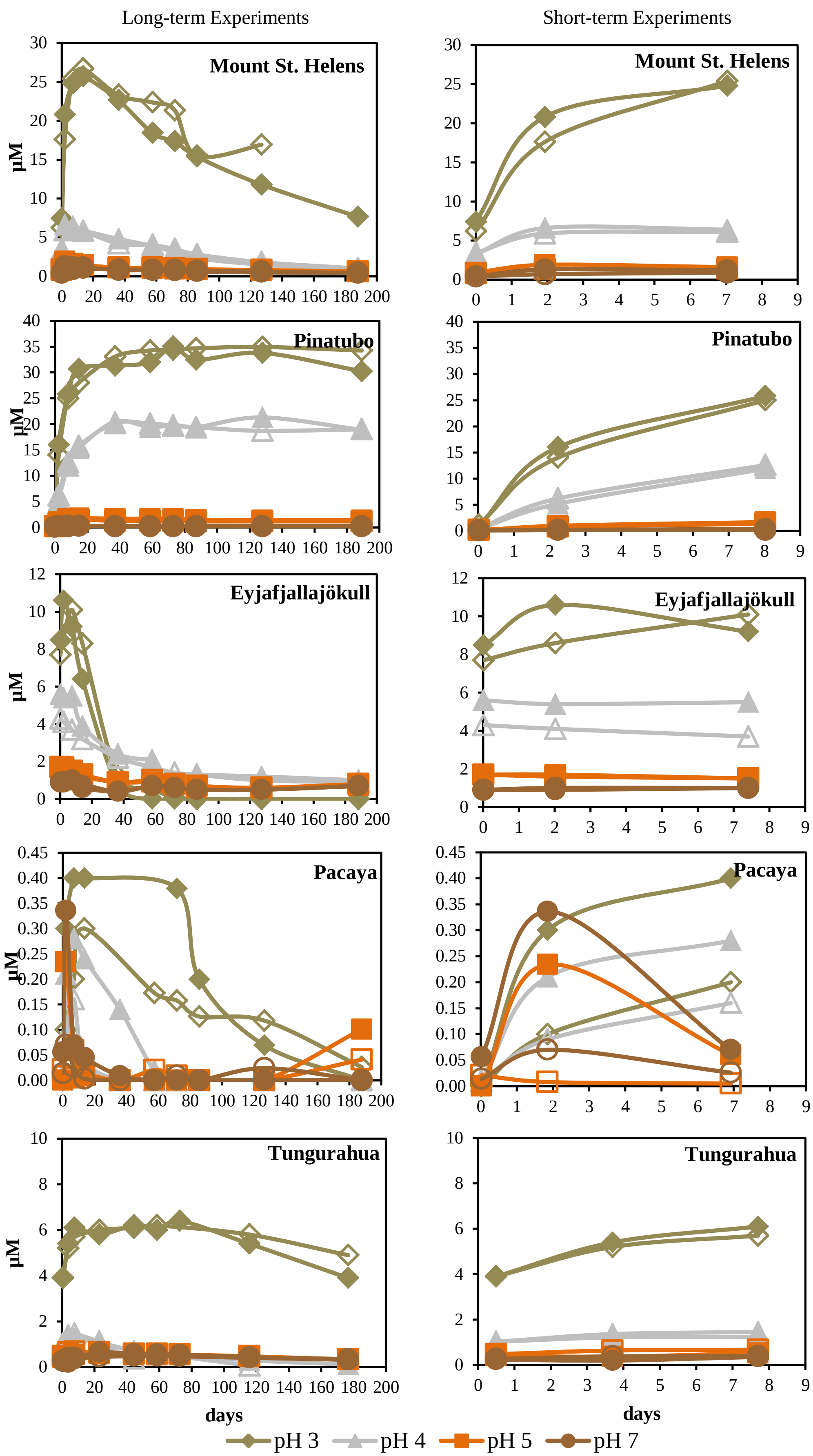

Fig. 9. PO_4 concentrations over time of volcanic ashes in solution ~pH 3, 4, 5, 7 with replicate experiments. Note different scales for each ash.

4.2.3 Phosphate release and Iron experimental analysis

General PO_4 trends are not unanimous, initial rapid release of PO_4 was followed by a change in concentrations (by the end of first to second week) that either increased slowly (Pinatubo), remained constant, or decreased slightly over time depending on the ash and pH (Fig. 9). Experimental dissolution and analysis of PO_4 release is complex. PO_4 release is dependent on the original solid phase composition and especially the solution chemistry including temperature, pH, and iron. Initial rapid release of PO_4 may be attributed to dissolution of apatite seen in the solid phase analysis of these ashes (undissolved in pre-dissolution phase and partially to fully dissolved in depleted solid phase) seen especially in Mount St. Helens and Pinatubo. Mount St. Helens' PO_4 concentrations begin to decrease slowly around ±25 days with final concentrations of ~8μM for pH 3 and ≤1μM for pH 4, 5, 7. Comparatively, Eyjafjallajökull ash rapidly decreases within 8 days and reaches concentrations of ≤1μM, with some concentrations below limit of detection (measuring below 0.0 ppm), by time sampling point eight. Pinatubo exhibits initial rapid release of concentrations followed by PO_4 concentrations remaining constant by time sampling point five. Interestingly, Pinatubo exhibits the greatest change in initial release yet has the lowest weight percent of phosphorous among other ashes. Slow and rapid decrease and constant concentrations in phosphate observed in these ashes may be attributed to precipitation of a secondary mineral, to phosphate speciation reaching equilibrium, or to absorption. Pacaya and Tungurahua ash show fairly low bulk concentrations of PO_4 and a decrease in concentrations over time.

The role of iron is significant in phosphate chemistry due to the pH dependency of iron solubility and Fe-phosphate speciation controlled by Fe^{2+} oxidizing easily to Fe^{3+} in solutions greater than pH 3. Therefore iron concentrations need to be considered when evaluating PO_4 concentrations in these ash dissolution experiments. Precipitation of an iron-phosphate mineral could be limiting dissolved phosphate concentrations in these experiments. This may be attributed from moderate to high weight percent of total Fe observed in bulk chemistry of the XRF data (Table 1), with the highest concentrations in Eyjafjallajökull, Pacaya, and Tungurahua (approximately ≥10%). Also, SEM analysis shows high amounts of Fe-Ti rich minerals seen in solid phase among the ashes. Dissolved iron analysis in later pH 4 batch experiments show low concentrations of total and ferrous iron with total iron greater than ferrous. Relatively high concentrations of total and ferrous iron are observed in final pH 3 ash solution (up to 46μM), excluding Tungurahua which has very low concentrations. Ferrous concentrations are similar to total Fe among the ashes in pH 3 solutions, however Fe^{2+} concentrations are lower in majority of samples of pH 4, 5, and 7. With the exception of Tungurahua, later pH 4 batch experiments' total and ferrous iron concentrations are comparatively higher (1-3 orders of magnitude) than total and ferrous iron concentrations measured in pH 4 solutions after 7 months (Table 3). Tungurahua's ash showed various Fe-rich hexagonal crystals and a relative high abundance of iron in XRF analysis compared to other ashes analyzed. The presence of an iron-phosphate precipitate is plausible as the cause of PO_4 decreases seen in solution chemistry with lower concentrations of Fe^{2+} observed in final solutions of pH 4, 5, and 7 (Fe^{2+} oxidizing to Fe^{3+}).

	Total Fe Concentrations		Ferrous Concentrations	
Sample name and pH	ppm	μM	ppm	μM
*Mount St. Helens, 4	0.22	4.02	0.21	3.75
*Mt. Pinatubo, 4	0.06	1.03	0.05	0.98
*Eyjafjallajökull, 4	0.11	2.05	0.10	1.89
*Pacaya, 4	0.04	0.80	0.04	0.67
*Tungurahua, 4	0.02	0.36	0.01	0.18
Mount St. Helens, 3	2.44	43.63	2.55	45.59
Mount St. Helens, 4	-	0.046	-	-
Mount St. Helens, 5	-	0.091	-	-
Mount St. Helens, 7	-	0.046	-	-
Mt. Pinatubo, 3	0.75	13.43	0.77	13.78
Mt. Pinatubo, 4	-	0.091	0.005	0.091
Mt. Pinatubo, 5	-	-	-	-
Mt. Pinatubo, 7	-	-	-	-
Eyjafjallajökull, 3	2.4	43.18	2.49	44.74
Eyjafjallajökull, 4	0.002	0.05	-	-
Eyjafjallajökull, 5	-	-	-	0.046
Eyjafjallajökull, 7	-	-	-	-
Pacaya, 3	2.19	39.21	2.24	40.15
Pacaya, 4	-	0.091	-	0.046
Pacaya, 5	-	-	-	-
Pacaya, 7	-	0.046	-	-
Tungurahua, 3	0.0945	1.70	0.02	0.36
Tungurahua, 4	0.057	1.03	0.057	1.023
Tungurahua, 5	-	0.046	-	-
Tungurahua, 7	0.02	0.36	0.013	0.22

Table. 3. Ferrozine analysis of secondary pH 4 batch experiments and final concentrations of primary batch experiments.
*Secondary pH 4 batch experiments, sampled after 11 days
-, Measured under limit of detection

4.2.4 Role of pH

For all major ions, total ion concentrations were pH dependent, with the greatest concentrations in pH 3 solution experiments and decreasing with increasing pH of all ashes (Tables A.1-A.5). Initial contact of volcanic ash with pH 7 solution resulted in an initial reduction in pH, which increases over sampling time period, except for the Eyjafjallajökull experiments. The Eyjafjallajökull ash sample shows the greatest change in pH, initially increasing an order of magnitude higher and then maintaining a pH ±1 order of magnitude of initial pH throughout experiment (Table A.3). In comparison, pH changes by dissolution experiments with Mount St. Helens, Pinatubo, Pacaya, and Tungurahua ashes are small (Tables A.1-A.2, A.4-A.5).

pH has proven to play a pivotal role in solution chemistry of the ashes, which is to be expected. Close inspection of Eyjafjallajökull, Mount St. Helens, and Pinatubo ash dissolution data suggests changes in pH may have contributed to changes in concentrations of phosphate and iron in solution (Fe^{2+} to Fe^{3+}). pH measurements are roughly constant or slightly increasing when PO_4 concentrations are approximately constant or slightly decreasing (see Discussion for more detail).

4.3 Dissolution rates

Si dissolution rates (**r**) are calculated as:

$$\mathbf{r}=\log\left(\mathbf{C}_{Si/t}\cdot\mathbf{V}/\mathbf{A}_i\cdot\mathbf{m}\right)$$

where $\mathbf{C}_{Si/t}$ designates the total aqueous Si concentrations of solution over time (slope calculation), $\mathbf{V}$ represents the volume of initial solutions of either pH 3, 4, 5, or 7, $\mathbf{A}_i$ is the specific surface area of the ash, where (i) corresponds to the method used to define the specific surface area (A_{BET}), and **m** is the mass of sample. Dissolution rates in this study have been normalized to mass and then to surface area with measured A_{BET} in order for comparison of past studies. Rates are shown as a function of pH at ~22°C (Fig. 10). Si was chosen for this study rather than including PO_4, Ca, or Mg rates in order to represent dissolution for the full time scale of experiments. The greatest Si dissolution rates observed were from Tungurahua ($\leq 2.4\text{x}10^{-4}$ μmol m^{-2} s^{-1}) followed by Pacaya ($\leq 5.4\text{x}10^{-5}$ μmol $^{-2}$ s^{-1}), then Mount St. Helens, Pinatubo, and Eyjafjallajökull. Tungurahua and Pacaya have the smallest BET specific surface area.

5. Discussion

This study has focused on the variation of dissolution kinetics of recent volcanic ash. Knowledge of the weathering rates of volcanic rocks and ash is important because weathering of Ca-Mg silicates and subsequent precipitation of Ca-Mg carbonates is a major control of atmospheric CO_2 over geological time (Walker et al., 1981; Berner., 1983; Berner and Kothavala, 2001; Wallmann, 2001; Berner, 2004; Gislason et al., 2009) and the only geologically long-term sink of atmospheric CO_2. Dissolution of some trace minerals, such as apatite, is also important because they release nutrients such as phosphate. These minerals have shown that it may influence the short-term carbon dioxide consumption and sequestration as biomass.

The ash dissolution experiments showed that concentrations of major ions in replicate batch experiments were generally reproducible for all ashes. The reacted solid phase of ashes exhibit distinctive dissolution features such as crystallographically-controlled etched pits on mineral surfaces, complete dissolution of surface minerals, and dissolved glassy phases that release major ions into solution, contributing to solution chemistry. Silicate dissolution studies have shown that the dissolution of glassy material is faster than that of its crystalline counterparts; basaltic rocks show fast dissolution than do Si-rich rocks (Wolff-Boenisch et al., 2006). However, this experimental work shows that many of the more crystalline phases appear to be more reacted than the glassy matrix. Although Si release is a controlling factor of solution chemistry, this study shows complex dissolution characteristics of PO_4, originating from apatite ($Ca_5(PO_4)_3OH$) that may contribute significantly to initial and final solution chemistry through the release of P nutrients and Ca into solution.

5.1 Si kinetics

Si release from the ash was a complex function of the chemical and mineralogical composition of the ashes and solution pH. Si dissolution increases linearly over time for all ashes with higher concentrations for each ash observed in more acidity (Fig. 8). It has been well documented that the dissolution of silicate glass is faster than its crystalline counterparts (Gíslason and Anórsson, 1990: Wolff-Boenisch et al., 2006). However, analysis of the ash samples by scanning electron microscopy show that the ash samples comprise both crystalline and glassy materials. Therefore, a comparison of silicate glass versus crystalline dissolution rates needs to be considered for this study. Observed Si release rates were normalized to BET surface area for a comparison to published mineral, rock, and glass dissolution rates. Si dissolution rates determined at an initial pH of 3 range over an order of magnitude, from $10^{-11.8}$ mol m^{-2} s^{-1} (Eyjafjalljökull) to $10^{-9.6}$ mol m^{-2} s^{-1} (Tungurahua). In comparison, in the pH 4 experiments, Si dissolution rates spanned two orders of magnitude from $10^{-12.3}$ mol m^{-2} s^{-1} (Eyjafjalljökull) to $10^{-10.3}$ mol m^{-2} s^{-1} (Tungurahua). Rates in pH 5 and pH 7 experiments are lower and vary slightly from pH 4 experimental dissolution rates (≤ 0.7 difference in magnitude), and both exhibit very similar rates with log rate of ±0.1 of a difference from one another. Si release rates from these ashes increase with increasing acidity. Calculated rates have a general trend: higher release rates for each ash with decreasing calculated BET surface area.

Fig. 10. Logarithm of dissolution rates versus pH of the ashes at ~22°C. Rates normalized to BET surface area. Dashed line represents *n* values of pH 3 and 4 experiments and their pH dependence of their dissolution rate. Solid shapes signify initial pH and unfilled shapes signify final pH of experiments. Note different vertical scales.

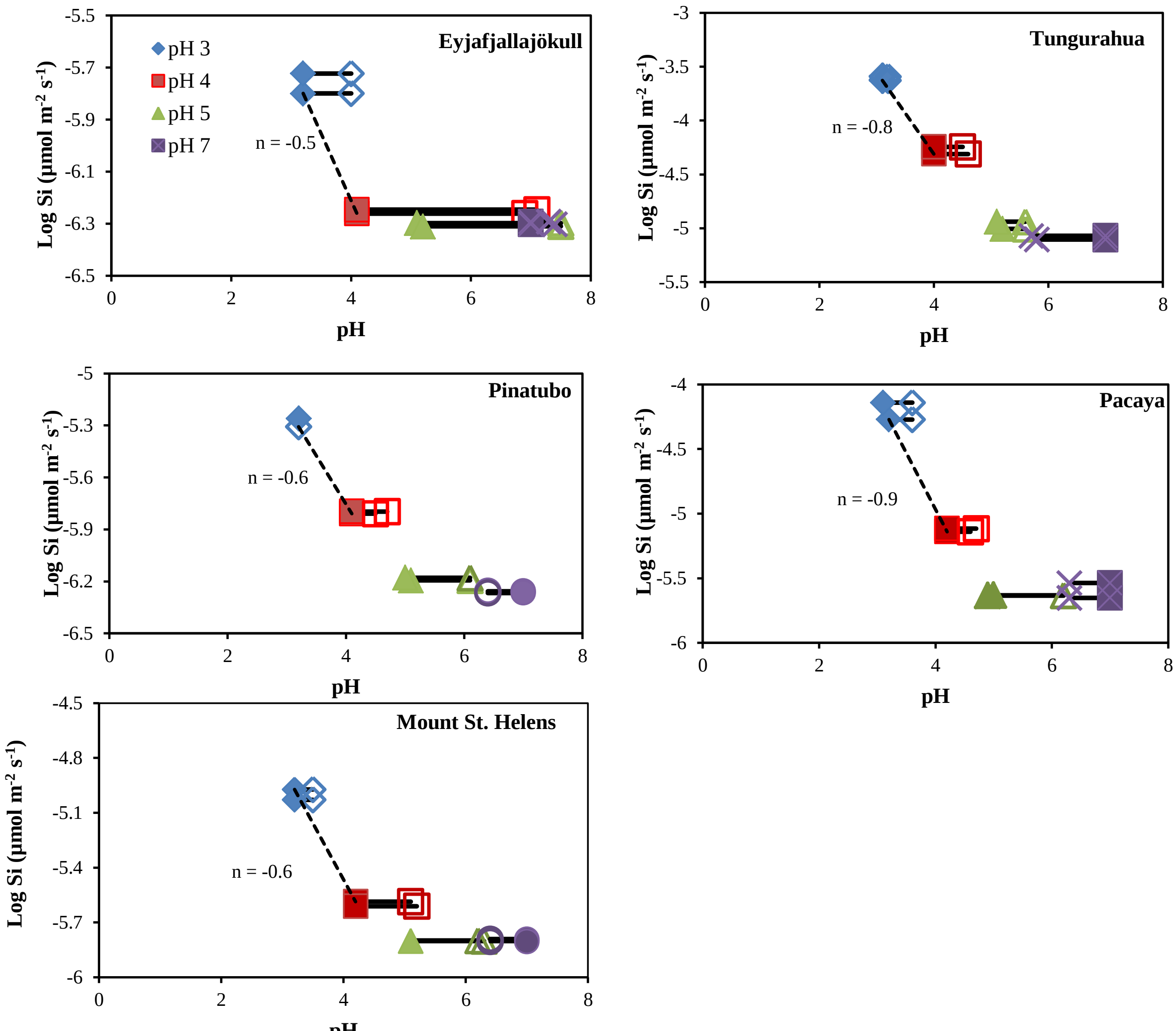

Rates measured in this study are compared to those for andesitic glass dissolution compiled by Wolff-Boenisch et al. (2004a). Reported rates are from 10^{-10} to 10^{-11} mol m^{-2} s^{-1} at pH 4 and 25°C, with their crystalline counterparts composing a wider range from 10^{-12} to 10^{-10} mol m^{-2} s^{-1} at pH 4 and 22-25°C (Cygan et al., 1989: Welch and Ullman ,1996). Other crystalline material such as high-end Si crystalline basalt dissolution rates have been recorded as high as $10^{-10.3}$ mol m^{-2} s^{-1} at pH 4 and 25°C (Gudbrandsson et al., 2011). Experimental results reported herein are generally equal to or lower than previous measured rates of both, andesitic silicate glass and crystalline andesite. Si dissolution rates determined herein suggest that both crystalline material and glass may be contributing to the overall Si release.

Si release from all ashes exhibits pH dependency, with largest rates from pH 3 solutions and rates decreasing with increasing pH (up to approximately pH 4-5) but reaction rates are relatively independent of acidity near neutral pH (pH ~ 5 to 8). These rates exhibit dissolution behavior of silicates similar to other studies; rates decrease with increasing pH at acidic conditions and increase with increasing pH at basic conditions (Blum and Lasaga, 1991: Welch and Ullman, 1993). A summary of all measured $\mathbf{r}_{Si, BET}$ are shown as a function of experimental pH (Fig. 10). The pH dependent dissolution of rate in acidic conditions can be described by $r = ka_{H+}^{n}$. The experimentally derived values of n determined from the pH 3 and 4 experiments ranges from ~-0.5 to -0.9. These values are higher than expected for a felsic glassy material. For example, the values of n for alkali feldspars range from -0.6 to -0.4 with a linear trend of pH versus temperature (Knauss and Wolery, 1986; Hellmann, 1994; Chen and Brantley, 2000). Dissolution rates of albite (a felsic and alkali feldspar mineral) reported by Chou & Wollast (1985) and Blum & Lasaga (1991) yielded n = ~-0.5 for pH < 7 at 25°C. In contrast, the pH dependence for dissolution of mafic minerals such as olivine and pyroxenes etc, tends to be higher, where n = -0.75 to -0.4 for pH < 7 with values increasing with increasing temperatures (Blum and Lasaga, 1988; Wogelius and Walther, 1991; Westrich et al., 1993; Chen and Brantley, 2000).

The dissolution rates calculated herein have some uncertainty stemming from the use of BET-normalized dissolution rates. Reported evidence shows BET surface areas of minerals change as a function of time and sample preparation prior to dissolution experiments (Brantley and Chen, 1995; Wolff-Boenisch et al., 2004). SEM analysis shows the presence of small glass fragments and crystalline silicate minerals post-experimental phase, suggesting that whole surface grain has not all reacted. Calculations were made to approximate Si content that was released into solution versus initial weight of ash grain in relation to weight percent. 2mg to 7mg of initial grains are the approximate weight of reacted material, with the most reaction revolving around the highest surface area measured, Eyjafjallajökull. However, this reacted material only makes up 0.2% - 0.7% of the total grain (originally 1g of ash material).This suggest that rates determined on a mass basis are more comparable than rates normalized to surface area. In the solid phase analysis, partial dissolution of Ca-Mg silicates were seen along with dissolution of felsic glass in all ashes, suggesting that total surface area is still undergoing reaction, and surface materials may be the factor controlling Si release into solution.

5.2 Ca and Mg release

The results in this study illustrate comparative dissolution behavior of divalent cations, specifically Ca and Mg and their influence to solution chemistry. The release of Ca and Mg ions into solution is an essential rate-limiting step for atmospheric CO_2 drawdown through the formation of Ca-Mg carbonates (Oelkers et al., 2008: Scheaf and McGrail, 2009: Gislason et al., 2009: Schaef et al., 2010: Gudbrandsson et al., 2011). Both Mg and Ca concentrations increase with increasing acidity and show relatively high initial releases. However, the initial release of Ca is significantly and distinctively higher than the initial release of Mg. Furthermore, final solutions show Mg concentrations are significantly lower than Ca concentrations in all pHs with magnesium release up to five times lower than calcium release (Eyjafjallajökull). This is in part due to the composition of the original ash samples which have Ca/Mg (mol/mol) of ~ 1.1 to 1.7, however the dissolved Ca/Mg molar ratios in solution at the end of the experiments range from ~ 2 to 100. Release of Mg in all pH 3 experiments is higher compared to Mg release in experiments of pH 4, 5, and 7. In the case of Ca release into solutions, pH 3 and 4 experiments exhibit relatively high concentrations compared to pH 5 and 7 experiments. Furthermore, Ca dominates in solution in contrast to other major ions. See Appendix A for graphs of major ions.

It seems likely that Mg release behavior stems from constituent mineral chemistry and glassy material of each volcanic ash. Evidence of Mg-rich minerals with compositions similar to forsterite olivine and pyroxenes were observed in SEM analysis. Previous studies have shown that magnesium is present in more rapidly dissolving minerals, such as olivine, which has specific dissolution rate ≥1 order of magnitude higher than that of Ca-rich minerals in acidic conditions (Wolff-Boenisch et al., 2006: Gudbrandsson et al., 2011). This suggests that significantly higher concentrations of calcium observed in solutions relative to concentrations of magnesium are coming from another solid phase source, such as apatite ($Ca_5(PO_4)_3(F,OH)$), soluble salts, and sulfides. Dissolution of these minerals would explain the general trend of high initial release of Ca in pH of ≤ 7 observed in all pH experiments. Evidence of the dissolution of crystalline apatite is shown in SEM analysis of Mount St. Helens, Pinatubo, and Eyjafjallajökull (Figs. 4-6). Substantial amounts of sulfide mineral phases, such as anhydrite and gypsum were present throughout Pinatubo's eruptive period (Bernard et al., 1991). However, the dissolution of glassy Ca containing phases and other minerals, such as pyroxenes and feldspars, cannot be excluded as sources of the high concentrations of Ca observed.

5.3 The complexity of phosphate behavior in experimental solutions

Phosphate release into solution plays particularly important geological and biological role in biogeochemical cycles. Dissolution of phosphate minerals, such as apatite, provides necessary nutrients to soils and organisms. Apatite is the most commonly occurring phosphate-bearing mineral in nature and is found as an accessory mineral in igneous rocks and metamorphosed limestones. Apatite can release P and Ca into solution to sequester atmospheric CO_2 (short term and long term) through the formation of calcium carbonates and as organic carbon according to the following reactions:

Geological:

$$\underbrace{Ca_5(PO_4)_3OH}_{\text{Apatite}} + 10CO_2 + 10H_2O \rightarrow 5Ca^{2+} + 10HCO_3^- + 3H_3PO_4 + H_2O$$

$$Ca^{2+} + 2HCO_3^- \rightarrow \underbrace{CaCO_3}_{\text{Calcite}} + CO_2 + 2H_2O$$

Biological: Redfield ratio

$$106CO_2 + 16NO_3^- + H_2PO_4^- + 122H_2O + 17H^+ \rightarrow C_{106}H_{263}O_{110}N_{16}P_1 + 138O_2$$

The weight percent oxide data from the XRF analysis show that PO_4 makes up approximately ≤1% of total bulk chemistry of these andesitic ashes (Table 1). In comparison, PO_4 concentrations in dissolution experiments contribute enormously to solution chemistry (Fig. 9). For example in the Mount St. Helens, Eyjafjallajökull, and Pinatubo experiments, PO_4 releases contribute approximately ~15-25% of the solutes relative to Si (Fig. 9). This suggests that phosphate mineral dissolution may play a vital role in total CO_2 consumption, not only through the dissolution of PO_4 and consumption of organic carbon, but through the dissolution of Ca-phosphate minerals that provides Ca into solution for long-term atmospheric CO_2 removal.

Although phosphate dissolution seems comparable to factors controlling atmospheric CO_2, it displays complex geochemical behavior in these ash dissolution experiments, depending on mineral reactivity and on solution composition. Nearly all of the experiments exhibit an initial (few hours to few days) rapid release of PO_4 to solution. Phosphate in solution then either increased more slowly, remained approximately constant, or actually decreased over time (Fig. 9). Solution pH was the overwhelming control of PO_4 release rate and PO_4 concentration (Fig. 11).

The general trend of phosphate is that concentrations decrease as pH increases, which reflects similar trends of the dissolution of apatite reported by Welch et al. (2002). In most experiments, initial phosphate release to solution is rapid. The change in PO_4 concentrations reflects both a consumption of protons and solution saturation with respect to the dissolving phase or possibly secondary mineral phases.

To understand previously determined phosphate trends, the role of pH and iron ionic behavior need to be understood. Change in pH may be directly affected by phosphate speciation from initial phosphate release and the rapid dissolution of surface glass and minerals, which both reflect consumption of protons and a general increase in pH (see section 5.1). As a result, these changes in pH may be driving iron oxidation reactions by initially releasing Fe^{2+} into solution. Ferrous iron minerals are more soluble in solution than ferric iron minerals. The rate of Fe oxidation is pH dependent; Fe^{2+} will readily oxidize to Fe^{3+} in solutions greater than pH 3. As pH changes, ferric iron can readily offer hydrogen or hydroxyl ions for cation or anion exchange. This suggest that available PO_4 ions may readily adsorb onto Fe^{3+} ions and produce potential for secondary mineral formation, such as strengite ($FePO_4$:$2H_2O$). In return, PO_4 concentrations in solution will decrease.

A comparison of the complexity of phosphate concentrations and its dissolution behavior in Pinatubo, Mount St. Helens, and Eyjafjallajökull solutions were examined at pH 3 and pH 4 at ~22°C (Fig. 11).

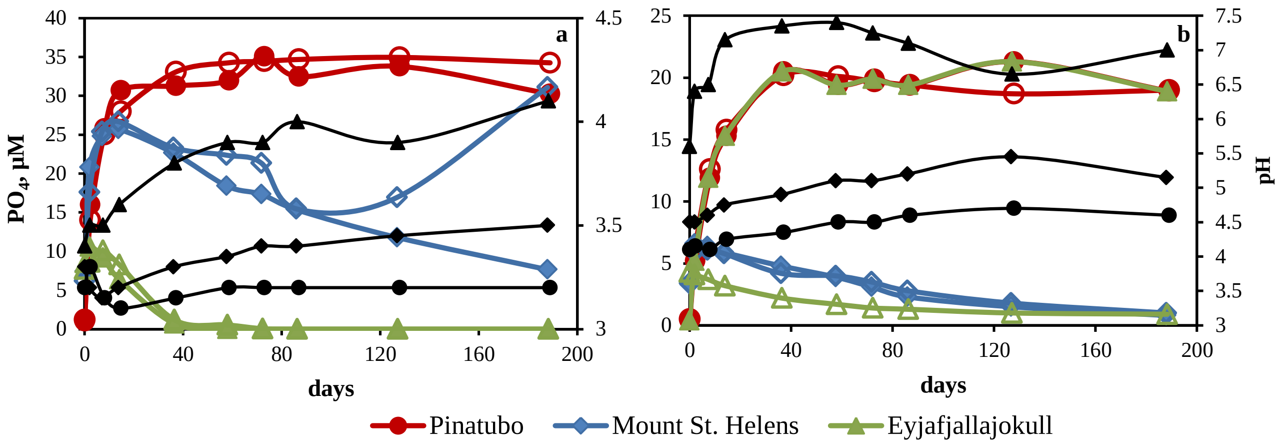

Fig. 11. PO_4 concentrations and affiliated replicate experiments in solution versus time of Pinatubo, Mount St. Helens, and Eyjafjallajökull ash. (a) pH 3 experiments, (b) pH 4 experiments. Black solid line represents average pH measurements of each experiment versus time. Associated shapes relate pH measurements with affiliated ash.

Pinatubo ash shows high initial PO_4 release (up to 16µM at pH 3) after 12 days and then concentrations remain approximately constant for the duration of the experimental time period. Changes in pH are small at both pH 3 and 4 experiments, pH 3 experimental initial and final pHs are the same, and pH 4 solution increases only from pH 4.1 to 4.6. Observations suggest that Pinatubo's solution chemistry may have reached equilibrium with respect to the dissolving phase and respect pH. pH 3 solutions maintained a low pH, suggesting that iron oxidation may have not played a primary role in the change of PO_4 concentrations. The solution pH of the pH 4 batch experiments were less acidic and contributed to the oxidization of Fe^{2+}, but iron dissolution was relatively low, suggesting that Fe^{3+} phases had little effect on total phosphate concentrations. However sorption and the formation of Fe-induced precipitates cannot be ruled out. SEM and XRF analysis shows evidence of iron-rich materials, which suggests adsorption and potential precipitation of an Fe-oxide, such as goethite, and an Fe-phosphate that may control solution saturation if present.

In comparison, Mount St. Helens shows highest initial phosphate release among the ashes (21µM at pH 3) and then a moderate decrease in concentrations for the duration of the time (Fig. 11). Changes in pH in experimental pH 3 and pH 4 solutions differ significantly from one another. pH 3 solutions only slightly changed over time, from 3.3 to 3.5, while pH change in pH 4 solutions changed about half of a magnitude more than initial pH values (4.5 to 5.2). The changes (both in concentration and pH) suggest that iron may be limiting phosphate release. pH 3 may be too acidic for 100% Fe^{2+} oxidation to occur. However, low concentrations of Fe^{3+} may be present, influencing a slow and moderate negative slope of PO_4 concentrations. pH 4 experiments and their affiliated pH changes create an ideal environment for fast iron oxidation reactions to occur and potential precipitation of secondary mineral phases. This would explain comparatively low initial phosphate concentrations in the pH 4 batch experiments and the decrease in concentration to near the limit of detection.

Eyjafjallajökull exhibits the most drastic changes in PO_4 concentrations and pH among the ashes. Observed pH changes of both pH 3 and pH 4 experiments were ±1 pH unit more than their corresponding initial pH (3.4 to 4.1 and 5.6 to 7.1). Highest initial concentrations of PO_4 from Eyjafjallajökull ash observed were in pH 3 solutions with ~11µM initially released after 8 days. However, both pH solutions and their initial PO_4^{3-} release were followed by a rapid decrease in concentrations to less than 1µM of dissolved phosphate by the end of the experiment. Rapid increase in pH suggests not only that dissolution of apatite play a role in pH change but also that silica glass and minerals had a significant affect in change in pH. In a reaction to pH changing quickly, iron oxidation may have occurred rapidly in solution, suggesting the formation of secondary minerals in solution and sorption of Fe^{3+} onto PO_4 from the presence of larger amounts of Fe^{3+} available in the initial phase of experiments. This is consistent with the determined Fe in the solid phase from XRF and SEM analyses.

In general, pH 5 and pH 7 experiments of all ashes display very low concentrations (≤5 µM in final solutions) of phosphate, suggesting that PO_4 release is low at near neutral pH conditions and the presence of phosphate sorption onto Fe-oxides in solution.

XRF and SEM data support this observation from moderate to high levels of Fe in the bulk solid phase. However, there are some uncertainties about other factors controlling dissolved phosphate release, such as biological removal of phosphate through adsorption. No analysis for the presence of organic material was conducted, but thorough observations were made with depleted solid phase, showing no conclusive evidence of biological activity on the ashes. Furthermore, the lack of dissolved iron analysis during the experimental time period provides no thorough conclusive evidence to solution reactions and solution chemistry towards iron concentrations in experiments.

PO_4 concentrations were observed for other ashes but proved less significant. Tungurahua and Pacaya have less comparable PO_4 dissolved concentrations with little changes in pH. These two ashes had high concentrations of Fe-oxides in the bulk solid phase, but these ashes show the smallest dissolved phosphate concentrations (Fig. 9). This suggest that observed high concentrations of iron recorded from XRF analysis and Fe-Ti rich minerals in solid phase, and the low Fe seen in ferrozine analysis may be originating from an Fe(III) mineral phase, which does not dissolve as easily as an Fe (II) mineral phase into solution.

5.4 Minerals: Reaction stoichiometry

Speciation and saturation state indices were determined using PHREEQC (Parkhurst and Appelo, 1999) to reflect reaction characteristics of minerals within the ashes using concentrations obtained from the 3rd and10th sampling event (Tungurahua: only 9th sampling event used), and using estimated (for 3rd sampling time) and measured ferrous concentrations (for 10th sampling time) from ferrozine analysis of solutions (Appendix, Table 1B & 2B). The Fe^{2+} concentration in solution was about ±1 order of magnitude higher at pH 3 than at pH 4 (Table 3). Fe^{3+} concentrations were assumed to be 1-2 orders of magnitude lower than measured ferrous concentrations. Most solutions are greatly undersaturated with respect to silicate minerals (e.g. pyroxenes, olivines), amorphous SiO_2, and hydroxyapatite. Stoichiometric calculations showed slight undersaturation of Ca/Fe-sulfates, Fe-phosphates, and Fe-hydroxides (amorphous and non-amorphous minerals), but super-saturated with respect to goethite (FeOOH) in all solutions. Although slight undersaturation of Fe-phosphates and Fe-hydroxides was seen from modeling, phases such as strengite and ferrihydrite form readily as metastable intermediates in acidic environments, and may have contributed to the decrease in phosphate due to the precipitation of an Fe-phosphate (Jones and Gislason, 2008).

Geochemical modeling reflects batch dissolution experiments. This suggests that the dissolution of glassy and mineral silicate phases play an active role for Ca, Mg, and Si concentrations. High dissolved concentrations of Ca and PO_4 may originate from the dissolution of apatite, salts, and sulfides. The role of iron through the dissolution of Fe(II) minerals and the formation of secondary minerals may play an important role, which directly relates to PO_4 behavior seen.

6. Conclusions

Dissolution behavior of Si, PO_4, Ca, and Mg of intermediate volcanic ashes shows relatively fast dissolution rates in comparison to previously determined basalt dissolution rates. The dissolution of andesitic to low-Si dacitic volcanic ash is complex. Both dissolution rates and extent of dissolution are controlled by mineralogical composition, solution chemistry and solution pH. Andesitic Si dissolution rates were similar to published basalt Si dissolution rates of glassy and crystalline material in previous studies. Both crystalline and glassy phases are contributing to Si release, with the majority of Si originating from the surface of the volcanic ash. Dissolution rates that are normalized to surface area are less comparable to each other than to rates normalized to mass. Initial high releases of PO_4 and Ca into solution through the dissolution of apatite suggest the importance of trace minerals to long-term and short-term atmospheric CO_2 removal as organic carbon and through the formation of carbonate minerals. Iron may play a key role in limiting phosphate release in the formation of secondary minerals.

Overall, the results suggests that in active tectonic regions where active volcanism occurs, such as HSIs or subduction zones, atmospheric CO_2 removal from the weathering of andesitic-dacitic ashes may be equally as important as from the weathering of andesitic-dacitic volcanic rocks and the weathering of basalts in these terrains. Furthermore, dissolution of recent andesitic-dacitic volcanic ashes may have potential not only for long-term removal of CO_2 but short-term removal of atmospheric CO_2 through the release of trace nutrients.

Recommendations for future work

Kinetics of water-rock interactions is strongly dependent on pH and temperature. Attempts to maintain room temperature and an initial homogenous pH of each solution prior to ash input were not entirely successful with some fluctuation in temperature of the laboratory and of initial solution varying ±0.1 of a difference in pH. Batch reactors that have prepared solutions at controlled pH and temperatures are strongly recommended to observe kinetics at these true pH and temperatures.

Although simulation of rock weathering may be difficult, flow-through experiments could be conducted in order to determine concentrations and fluxes of elements in the ash at different controlled pH and temperatures. Analyses of iron concentrations and phases in solution should be measured throughout experiments.

Furthermore, sampling periodically and more frequently during the initial phase of the dissolution experiments would produce more thorough results (i.e. within the first 12-24 hours from the start of dissolution experiments). Furthermore, sampling over longer time periods would show equilibrium and/or saturation with respect to mineral phases in solution.

Determination of ash mineralogy by x-ray diffraction would aid interpretation of SEM, XRF, solution chemistry and geochemical modeling. Determined dissolution rates in this study have shown that normalizing to surface area may or may not be a true representation of the determined dissolution rates due to the varying ash particle sizes and surface dissolution. Analysis of similar measured A_{BET} surface areas through sieving suggests that a better comparison of ash dissolution and therefore dissolution rates would be determined from dissolution experiments.

References Cited

Aller, R.C., 1998. Mobile deltaic and continental shelf muds as suboxic, fluidized bed reactors. Mar. Chem. 61, 143-155.

Amiotte-Suchet, P., Probst, J., Ludwig, W., 2003. Worldwide distribution of continental rock lithology: implications for the atmospheric/soil CO_2 uptake by continental weathering and alkalinity river transport to the oceans. Glob. Biogeochem Cycl. 17, 1038. Doi: 10, 1029/2002GB001891.

Bernard, A., Demaiffe, D., MattielliN., Punongbayan, R., 1991. Anhydrite-bearing pumices from Mount Pinatubo- Further evidence for the existence of sulfur-rich silicic magmas. Nature 354 (6349), 139-140.

Berner, R.A., Lasaga, A.C., Garrels, R.M., 1983. The carbonate-silicate geochemical cycle and its effect on atmospheric carbon dioxide over the past 100 million years. Am. J. Sci. 283, 641-683.

Berner, R.A., 1999. A new look at long-term carbon cycle. GSA Today 9, 2-6.

Berner, R., Kothavala, Z., 2001. GEOCARB III: A revised model of atmospheric CO_2 over Phanerozoic time. Am. J. Sci. 301, 182-204.

Berner, R., 2004. The Phanerozoic carbon cycle: CO_2 and O_2. The Phanerozoic carbon cycle:CO_2 and O_2. i-viii, 1-150.

Bernstein, R., Baxter, P., Falk, H., Ing, P., Foster, L., Frost, F., 1986.Immediate Public Health Concerns and Actions in Volcanic Eruptions: Lessons from the Mount St. Helens Eruptions, May 18-October 18, 1980. Am. J. Public Health 76, Supplement.

Biggs, J., Mothes, P., Ruiz, M.,Amelung, F., Dixon, T., Baker, S., Hong, S., 2010. Stratovolcano growth by co-eruptive intrusion: The 2008 eruption of Tungurahua Ecuador. Geophys. Res. Lett.37, Number: L21302 DOI: 10.1029/2010GL044942.

Blum, A., and Lasaga, A.C. (1988) Role of surface speciation in the low temperature dissolution of minerals. Nature 33 l, 4ll-433.

Blum, A., Lasaga, A., 1991. The role of surface speciation in the dissolution of albite. Geochim. Cosmochim. Acta 55, 2193-2201.

Brantley, S., Chen, Y., 1995. Chemical weathering rates of pyroxenes and amphiboles. Rev. Min. 31, 119-172.

Brunauer, S., Emmett, P.,Teller, E., 1938. Adsorption of gases in multimolecular layers. Journal of the American Chemical Society 60, 309-319.

Carlsen, H., Gislason, T.,Benediktsdottir, B., Kolbeinsson, T., Hauksdottir, A., Thorsteinsson, T., Briem, H., 2012. A survey of early health effects of the Eyjafjallajokull 2010 eruption in Iceland: a population-based study. British Medical Journal 2 (2) e000343.

Cashman, K., McConnell, S., 2005. Multiple levels of magma storage during the 1980 summer eruptions of Mount St. Helens, WA. Bull Vocanol. 68, 57-75.

Chen, Y., Brantley, S., 2000. Dissolution of forsteritic olivine at 65°C and 2 < pH < 5.Chemical Geology 165, 267-281.

Chou, L., Wollast, R., 1985. Steady-state kinetics and dissolution mechanisms of albite. Am. J. Sci. 285, 963-993.

CNN web, "Volcano known as "Throat of Fire" erupts in Ecuador. http://edition.cnn.com/2010/WORLD/americas/12/04/ecuador.volcano/. (04.20.12)

Conway, M., Diehl, J., Matias, O., 1992. Paleomagnetic contraints on eruption patterns at the Pacaya composite volcano, Guatemala. Bull. Volcanol. 55, 25-32.

Cygan, R., Casey, W., Boslough, M., Westrich, H., Carr, M., Holdren, G., 1986. Dissolution kinetics of experimentally shocked silicate minerals. Chemical Geology 78, 229-244.

Dalton, M., Waite, G.,Watson, M., Nadeau, P., 2010. Multiparameter quantification of gas release during weak Strombolian eruptions at Pacaya Volcano, Guatemala. Geophys. Res. Lett. 37
Article Number: L09303, DOI: 10.1029/2010GL042617.

Dellino, P., Gudmundsson, M., Larsen, G., Mele, D., Stevenson, J., Thordarson, T., Zimanowski, B.,2012. Ash from the Eyjafjallajokull eruption (Iceland): Fragmentation processes and aerodynamic behavior. J. Geophys. Res. Solid Earth 117, Article Number: B00C04 DOI: 10.1029/2011JB008726.

De la Cruz-Reyna, S., Tarraga, M., Ortiz, R., Martinez-Bringas, A., 2010. Tectonic earthquakes triggering volcanic seismicity and eruptions. Case studies at Tungurahua and Popocatepetl volcanoes.J. Vol. Geotherm. Res.193, 37-48.

de Hoog, J., Hattori, K., Hoblitt. R., 2003. Oxidized sulfur-rich mafic magma at Mount Pinatubo, Philippines. Contributions of Mineralogy and Petrology. 146, 750-761.

Dessert, C., Dupré, B., Gaillerdet, J., Francois, L., Allégre, C.J., 2003. Basalt weathering laws and the impact of basalt weathering on the global carbon cycle. Chem Geol. 202, 257-273.

Di Muro, A., Pallister, J., Villemant, B., Newhall, C., Michel, S., 2008. Pre-1991 sulfur transfer between mafic injections and dacite magma in Mt. Pinatubo reservoir.. J. Volcan Geotherm. Res.175. 517-540.

Duggen, S., Croot, P., Schacht, U., Hoffmann, L., 2007. Subduction zone volcanic ash can fertilize the surface ocean and stimulate phytoplankton growth: Evidence from biogeochemical experiments and satellite data. Geophys. Res. Lett. 34(5), L01612, doi: 10.1029/2006GL027522.

Duggen, S., Olgun, N., Croot, P., Hoffman, L., Dietze, H., Delmelle, P., and Teschner, C., 2010. The role of airborne volcanic ash for the surface ocean biogeochemical iron-cycle: a review. Biogeosciences 7, 827-844.

Eychenne, J., Le Pennec, J.L., Troncoso, L., Gouhier, M., Nedelec, J.M., 2012. Causes and consequences of bimodal grain-size distribution of tephra fall deposited during the August 2006 Tungurahua eruption (Ecuador). Bull. Volcan. 74, 187-205.

Fero, J., Carey, S., Merrill, J., 2008. Simulation of the 1980 eruption of Mount St. Helens using the ash-tracking model PUFF. J. Volcan. Geotherm. Res. 175, 355-366.

Farlow, N., Oberbeck, V., Snetsinger, K., Ferry, G., Polkowski, G., Hayes, D., 1981. Size Distributions and Mineralogy of Ash Particles in the Stratosphere from Eruptions ofMount St. Helens. AAAS. 211, No. 4484, 832-834.

Gaillardet, J., Dupré, B., Louvat, P., Allégre, C.J., 1999. Global silicate weathering and CO_2 consumption rates dissolved from the chemistry of large rivers. Chem. Geol. 159, 3-30.

Gislason, S., Anorsson, S., 1990. Saturation state of natural waters in Iceland relative to primary and secondary minerals in basalts.

Gislason, S., Oelkers, E., 2003. The mechanism, rates and consequences of basaltic glass dissolution: II. An experimental study of the dissolution rates of basaltic glass as a function of pH and temperature. Geochim. Cosmochim. Acta 67, 3817-3832.

Gislason, S.,Oelkers, E., Eiriksdottir, E., Kardjilov, M., Gisladottir, G., Sigfusson, B., Snorrason, A., Sverrir, E., Hardaottir, J., Torssander, P., Oskarsson, N. . 2009. Direct evidence of the feedback between climate and weathering. Earth Planet. Sci. Lett. 277, 213-222.

Gislason, S., Alfredsson H., 2010. Sampling the Volcanic Ash from the Eyjafjallajokull Volcano, Iceland- A Personal Account. Elements 4, 269-270.

Gislason, S., Alfredsson, H., Eirikdottir, E., Hassenkam, T., Stipp, S., 2011. Volcanic ash from the 2010 Eyjafjallajökull eruption. Applied Geochem. 26, 5188- 5190.

Goldsmith, S., Carey, A., Lyons, W., Hicks, M., 2008. Geochemical fluxes and weathering on high standing islands: Taranaki and Manawatu-Wanganui Regions, New Zealand. Geochim Cosmochim. Acta 72 (9), 2248-2267.

Goldsmith, S., Carey, A., Johnson, B., Welch, S., Lyons, W., McDowell, W., Pigott, J., 2010. Stream geochemistry, chemical weathering and CO_2 consumption potential of andesitic terrains, Dominica, Lesser Antilles. Geochim. Cosmochim. Acta 74, 85-103.

Gomez, R., Rose, W., Palma, J., Escobar, R., 2012. Notes on a Map of the 1961–2010 Eruptions of Volcán de Pacaya, Guatemala. Geological Society of America. In: GSA Digital Map and Chart Series 10.

Gudbrandsson, S., Wolff-Boenisch, D., Gislason, S., Oelkers, E., 2011. An experimental study of crystalline basalt dissolution from $2 \leq$ pH ≤ 11 and temperatures from 5 to 75°C. Geochim. Cosmochim. Acta 75, 5496-5509.

Hall, M., Robin, B., Beate, B., Mothes, P., Monzier, M., 1999. Tungurahua Volcano, Ecuador: structure, eruptive history and hazards. J. Vol. Geotherm. Res.91, 1-21.

Hellmann, R., 1994. The albite–water system: Part I. The kinetics of dissolution as a function of pH at 100, 200, and 3008C. Geochim. Cosmochim. Acta 58, 595–611.

Jones, M., Gislason, S., 2008. Rapid releases of metal salts and nutrients following the deposition of volcanic ash into aqueous environments. Geochim. Cosmochim. Acta 72, 3661-3680.

Keiding, J., Sigmarsson, O., 2012. Geothermobarometry of the 2010 Eyjafjallajokull eruption: New constraints on Icelandic magma plumbing systems. J. Geophys. Res.-Solid Earth 117, Article Number: B00C09.

Knauss, I.G., and Wolery, T.J.,1986. Dependence of albite dissolution kinetics on pH and time at 25’C and 70 'C. Geochimica et Cosmochimica Acta 50, 2481-2497.

Labat, D., Goddéris, Y. Probst, J.L., Guyot, J.L., 2004. Evidence for global runoff increase related to climate warming. Adv. Water Resour 27, 631-642.

Langmann, B., Zaksek, K., Hort, M., Duggen, S., 2010. Volcanic ash as fertilizer for the surface ocean. Atmos. Chem. Phys. Discuss. 10, 711-734.

Lasaga, A., Soler, J., Ganor, J., Burch, T., Nagy, K., 1994. Chemical-weathering rate laws and global geochemical cycles. Geochim. Cosmochim Acta 58, 2361- 2386.

Le Pennec, J., Jaya, D., Samaniego, P., Ramón, S., Moreno, Y., Egred, Y., van der Plicht, J., 2008. The AD 1300 1700 eruptive periods atTungurahua volcano, Ecuador, revealed by historical narratives, stratigraphy and radiocarbon dating. J. Volcanol. Geotherm. Res.176, 70–81.

Lockwood, J., Hazlett, R., 2010. Volcanoes: Global Perspectives. UK: John Wiley and Sons Inc.

Louvat, P., Allegre, C., 1997. Present denudation rates on the island of Reunion determined by river geochemistry: basalt weathering and mass budget between chemical and mechanical erosions. Geochim. Cosmochim Acta 61, 3645-3669.

Lyons, W., Carey, A., Hicks, D., Nezat, C., 2005. Chemical weathering in high-sediment-yielding watersheds, New Zealand. J. Geophys. Res. 110(FO1008). doi: 10.1029/2003JF000088.

Meybeck, M., 1987. Global chemical weathering of surficial rocks estimated from river dissolved loads. Am. J. Sci. 287, 401-428.

Navarra-Stichler, A., Brantley, S., 2007. Basalt weathering across scales. Earth Planet Sci. Lett. 261, 321-334.

Newhall, Christopher, and Raymundo Punongbayan. Fire and mud. Univ of Washington Pr, 1996.

Oelkers, E., Gislason, S., Matter, J., 2008. Mineral carbonation of CO_2. Elements 4, 333-337.

Ongaro, T., Widiwijayanti, C., Clarke, A., Voight, B., Neri, A., 2011. Multiphase-fl ow numerical modeling of the 18 May 1980 lateral blast at Mount St. Helens, USA. Geological Society of America.

Pallister, J., Hoblitt, R., Reyes, A., 1992. A basalt trigger for the 1991 eruptions of Pinatubo volcano?. Nature. 356.2, 426-428.

Parkhurst, D.L. and Appelo, C.A.J., 1999. User's guide to PHREEQC (version 2) - a computer program for speciation, reaction-path, 1D-transport, and inverse geochemical calculations. US Geol. Surv. Water Resour. Inv. Rep. 99-4259, 312p.

Pierson, T., Janda, R., Umbal, J., Daag, J., 1992. Immediate and long-tern hazards from lahars and excess sedimentation in rivers draining mt. pinatubo, philippines. vancouver: us geological survey, 1-8.

Rad, S., Louvat, P., Gorge, C., Gaillardet, J., Allegre, C., 2006. River dissolved and solid loads in the Lesser Antilles: New insight into basalt weathering processes. J. Geochem. Ex. 88, 308-312

Rodriguez, L.,Watson, I., Rose, W., Branan, Y., Bluth, G., Chigna, G., Matias, O., Escobar, D., Carn, S., Fischer, T., 2004. SO_2 emissions to the atmosphere from active volcanoes in Guatemala and El Salvador, 1999-2002.J. Volcan. Geotherm Res. 138, 325, 344.

Ruiz, M., Lees, J., Johnson, J., 2006. Source constraints of Tungurahua volcano explosion events, Bull. Volcanol. 68, 480–490.

Santelli, C., Welch, S., Westrich, H., Banfield, J., 2001. The effect of Fe-oxidizing bacteria on Fe-silicate mineral dissolution. Chemical Geology 180, 99- 115.

Sarmiento, J., 1993. Atmospheric CO_2 stalled. Nature 365, 697-698.

Schaef, H., McGrail, B., 2009. Dissolution of Columbia River basalt under mildly acidic conditions as a function of temperature: experimental results revelant to the geological sequestration of carbon dioxide. Appl. Cosmochim. Acta 24, 980-987.

Schaef, H., McGrail, B., Owen A., 2010. Carbonate mineralization of volcanic province basalts. Int. J. Greenhouse Gas Control 4, 249-261.

Schmincke, H., 2004. Volcanism, Springer-Verlag, Berlin Heidelberg New York, 324.

Schopka, H., Derry, L., Arcilla, C., 2011. Chemical weathering, river geochemistry and atmospheric carbon fluxes from the volcanic and ultramafic regions on Luzon Island, the Philippines. Geochim. Cosmochim. Acta 75, 978-1002.

Scripps CO_2. Atmospheric CO_2. 2012. http://scrippsco2.ucsd.edu/research/atmospheric_co2.html.

Stohl, A., Prata, A., Eckhardt, S., Clarisse, L., Durant, A., Henne, S., Kristiansen, N., Minikin, A., Schumann, U., Seibert, P., Stebel, K.,Thomas, H., Thorsteinsson, T.,Weinzierl, B., 2011. Determination of time- and height-resolved volcanic ash emissions and their use for quantitative ash dispersion modeling: the 2010 Eyjafjallajokull eruption . Atmos. Chem. Phys. 11 (9), 4333-4351.

Stookey, L., 1970. Ferrozine-A new spectrophotometric reagent for iron. Analytical Chemistry 42, 79-81.

Thorsteinsson, T., Johannsson, T., Stohl, A., Kristiansen, N., 2012. High levels of particulate matter in Iceland due to direct ash emissions by the Eyjafjallajokull eruption and resuspension of deposited ash. J. Gephys. Res. –Solid Earth 117, Article Number: B00C05.

U.S. Geological Survey, 2005. Fact Sheet: Mount St. Helens -From the 1980 Eruption to 2000. http://pubs.usgs.gov/fs/2000/fs036-00/.

Walker, J.C.G., Hays, P.B., Kasting, J.F., 1981. A negative feedback mechanism for the longterm stabilization of the Earth's surface temperature. J. Geophys. Res. 86, 9776-9782.

Wallmann, K., 2001. Controls on the Cretaceous and Cenozoic evolution of seawater composition, atmospheric CO_2 and climate. Geochim Cosmochim Acta 65, 2469-2485.

Welch, S., Ullman, W., 1993. The effect of soluble organic acids on feldspar dissolution rates and stoichiometry. Geochim. Cosmochim. Acta 57: 2725- 2736.

Welch, K., Lyons, W., Graham, E., Neumann, J., Thomas, J., Mikesell, D., 1996. Determination of major element chemistry in terrestrial waters form Antarctica by ion chromatography. J. Chromatogr. A 739, 256-263.

Welch, S., Ullman, W., 1996. Feldspar dissolution in acidic and organic acid solutions: Compositional and pH dependence of dissolution rate. Geochim. Cosmochim. Acta 60.

Welch, S., Taunton, A., Banfield J., 2002. Effect of Microorganisms and Microbial Metabolites on Apatite Dissolution. Geomicrobiology Journal 19, 343-367.

Westrich, H., Cygan, R., Casey, W., Zemitis, C., Arbold, G., 1993. The dissolution kinetics of mixed-cation orthosilicate minerals. Am. J. Sci. 293, 869–893.

Wogelius, R.A., Walther, J.V., 1991. Olivine dissolution at 258°C: Effects of pH, CO_2, and organic acids. Geochim. Cosmochim. Acta 55, 943–954.

Wolff-Boenisch, D., Gislason, S., Oelkers, E., 2004a. The dissolution rates of natural glasses as a function of their composition at pH 4 and 10.6, and temperatures from 25 to 74°C. Geochim. Cosmochim. Acta 68, 4843-4582.

Wolff- Boenisch, D., Gislason, S., Oelkers, E., 2006. The effect of crystallinity on dissolution rates and CO_2 consumption capacity of silicates. Geochim. Cosmochim. Acta70, 858-870.

Appendix (A)

Compilations of concentrations of dissolved major ions in solutions ~pH 3, 4, 5, 7

Appendix (B)

Compilation of primary and secondary mineral phases from PHREEQC geochemical modeling

Table A.1 Dissolved concentrations of Mount St. Helens ash

Sample number	Sampling date	pH	A_{BET} (m^2/g)	Si (ppm)	Li (ppm)	Na (ppm)	K (ppm)	Mg (ppm)	Ca (ppm)	F (ppm)	Cl (ppm)	SO_4 (ppm)	PO_4 (ppm)
3A	22-Feb-11	3.3	0.783	0.191	0.000	1.399	0.632	0.163	1.585	0.122	36.668	0.348	0.699
3A	24-Feb-11	3.2	0.783	1.953	—	0.571	0.520	0.247	2.741	0.091	34.763	0.272	1.974
3A	1-Mar-11	3.2	0.783	3.929	0.000	0.668	0.711	0.461	3.195	0.121	36.482	0.407	2.355
3A	8-Mar-11	3.2	0.783	2.258	0.000	0.952	0.651	0.451	3.588	0.122	34.868	0.508	2.445
3A	30-Mar-11	3.3	0.783	4.405	0.000	0.808	0.783	0.936	2.671	0.149	36.057	0.169	2.152
3A	21-Apr-11	3.4	0.783	6.601	0.000	0.903	0.685	1.188	2.688	0.151	35.673	0.274	1.750
3A	5-May-11	3.4	0.783	7.684	0.001	0.973	0.742	1.360	2.717	0.163	36.506	0.373	1.648
3A	19-May-11	3.4	0.783	8.470	0.001	1.175	0.837	1.456	2.744	0.159	36.030	0.411	1.460
3A	29-Jun-11	3.5	0.783	11.046	0.001	1.174	0.833	2.306	5.065	0.161	39.645	0.733	1.120
3A	29-Aug-11	3.5	0.783	15.162	0.001	1.291	0.830	2.494	5.195	0.157	39.059	0.977	0.727
3B	22-Feb-11	3.3	0.783	0.159	—	0.336	0.251	0.132	1.162	0.028	35.328	0.229	0.585
3B	24-Feb-11	3.2	0.783	0.660	—	0.303	0.300	0.182	2.788	0.086	34.861	0.384	1.673
3B	1-Mar-11	3.1	0.783	1.453	0.000	0.384	0.364	0.465	2.906	0.129	35.548	0.213	2.413
3B	8-Mar-11	3.2	0.783	2.266	0.000	0.488	0.374	0.422	3.495	0.132	36.451	0.152	2.538
3B	30-Mar-11	3.3	0.783	4.199	0.000	0.548	0.446	0.912	2.584	0.155	35.508	0.244	2.217
3B	21-Apr-11	3.3	0.783	6.312	0.001	0.706	0.510	1.179	2.694	0.158	35.688	0.289	2.125
3B	5-May-11	3.4	0.783	7.421	0.001	0.823	0.573	1.323	2.732	0.161	36.275	0.465	2.028
3B	19-May-11	3.4	0.783	8.318	0.001	0.822	0.515	1.367	2.714	0.157	35.348	0.440	1.470
3B	29-Jun-11	3.4	0.783	11.163	0.001	0.888	0.590	2.277	4.967	0.167	39.187	0.018	1.608
3B	29-Aug-11	3.5	0.783	6.927	0.001	0.981	0.581	2.432	5.136	0.174	38.656	1.072	2.954
4A	22-Feb-11	4.5	0.783	0.082	—	1.020	0.388	0.124	0.951	0.040	3.501	0.332	0.315
4A	24-Feb-11	4.5	0.783	3.513	—	0.669	0.246	0.172	1.389	0.025	3.342	0.198	0.627
4A	1-Mar-11	4.6	0.783	5.676	0.000	0.616	0.222	0.232	1.339	0.027	3.392	0.315	0.605
4A	8-Mar-11	4.8	0.783	0.702	—	0.971	0.052	0.210	1.450	0.035	3.286	0.201	0.562
4A	30-Mar-11	4.9	0.783	1.145	0.000	0.502	0.284	0.184	1.188	0.031	3.401	0.290	0.453
4A	21-Apr-11	5.1	0.783	1.684	0.000	0.981	0.055	0.182	1.151	0.048	3.538	0.346	0.372

4A	5-May-11	5.1	0.783	1.965	0.000	1.046	0.048	0.177	1.109	0.043	3.509	0.344	0.290
4A	19-May-11	5.2	0.783	2.396	0.000	1.170	0.059	0.192	1.072	0.062	3.466	0.389	0.214
4A	29-Jun-11	5.5	0.783	2.966	0.000	1.065	0.045	0.377	0.943	0.076	3.620	0.618	0.146
4A	29-Aug-11	5.1	0.783	3.928	0.000	1.166	0.048	0.330	0.998	0.091	3.694	0.976	0.075
4B	22-Feb-11	4.5	0.783	0.076	–	2.038	0.134	0.130	1.020	0.162	3.763	0.338	0.327
4B	24-Feb-11	4.5	0.783	0.279	–	0.334	0.251	0.155	1.302	0.027	3.387	0.195	0.559
4B	1-Mar-11	4.6	0.783	0.529	0.000	0.354	0.308	0.212	1.276	0.028	3.337	0.239	0.577
4B	8-Mar-11	4.8	0.783	0.694	–	0.682	0.204	0.206	1.420	0.032	3.367	0.188	0.548
4B	30-Mar-11	4.9	0.783	1.152	0.000	0.423	0.342	0.180	1.202	0.029	3.429	0.214	0.400
4B	21-Apr-11	5.1	0.783	1.730	0.000	0.648	0.261	0.225	1.764	0.054	3.575	0.591	0.379
4B	5-May-11	5.1	0.783	2.023	0.000	0.681	0.228	0.205	1.326	0.038	3.544	0.388	0.331
4B	19-May-11	5.2	0.783	2.352	0.000	0.870	0.224	0.208	1.325	0.040	3.609	0.443	0.270
4B	29-Jun-11	5.4	0.783	3.093	0.000	0.738	0.205	0.297	1.193	0.036	3.780	0.630	0.173
4B	29-Aug-11	5.2	0.783	4.081	0.000	0.746	0.133	0.383	1.177	0.045	3.624	0.853	0.093
5A	22-Feb-11	5.9	0.783	0.057	–	0.550	0.013	0.101	0.800	0.032	0.479	0.595	0.084
5A	24-Feb-11	6.0	0.783	6.449	–	0.443	0.034	0.101	0.442	0.007	0.464	0.246	0.183
5A	1-Mar-11	6.0	0.783	9.302	–	0.323	0.110	0.146	0.635	0.008	0.563	0.309	0.151
5A	8-Mar-11	6.2	0.783	0.320	–	0.556	0.025	0.110	0.622	0.013	0.491	0.281	0.137
5A	30-Mar-11	6.2	0.783	0.680	–	5.838	0.136	0.032	0.173	0.272	5.659	0.300	0.104
5A	21-Apr-11	6.1	0.783	0.902	0.000	0.497	0.084	0.126	0.605	0.019	0.510	0.293	0.096
5A	5-May-11	6.1	0.783	1.090	0.000	0.432	0.090	0.122	0.619	0.017	0.591	0.381	0.089
5A	19-May-11	6.1	0.783	1.319	0.000	0.542	0.150	0.127	0.603	0.015	0.743	0.502	0.082
5A	29-Jun-11	6.5	0.783	1.799	0.000	0.422	0.087	0.212	0.995	0.028	0.486	0.717	0.067
5A	29-Aug-11	6.2	0.783	2.498	0.000	0.498	0.100	0.223	1.066	0.015	0.486	0.917	0.054
5B	22-Feb-11	5.8	0.783	0.042	–	0.960	0.021	0.226	1.391	0.085	0.639	0.197	0.080
5B	24-Feb-11	5.9	0.783	0.129	–	0.337	0.061	0.154	0.853	0.009	0.469	0.356	0.121
5B	1-Mar-11	6.0	0.783	0.238	–	0.253	0.113	0.156	0.763	0.008	0.473	0.381	0.128
5B	8-Mar-11	6.1	0.783	0.297	–	0.447	0.024	0.115	0.700	0.009	0.453	0.280	0.136
5B	30-Mar-11	6.2	0.783	0.563	0.000	0.400	0.036	0.100	0.507	0.012	0.458	0.236	0.109
5B	21-Apr-11	6.1	0.783	0.891	0.000	0.395	0.191	0.116	0.605	0.016	0.521	0.431	0.101
5B	5-May-11	6.1	0.783	1.088	0.000	0.368	0.164	0.120	0.605	0.012	0.489	0.372	0.094

5B	19-May-11	6.2	0.783	1.268	0.000	0.567	0.118	0.131	1.446	0.020	0.528	0.401	0.086
5B	29-Jun-11	6.5	0.783	1.796	0.000	0.359	0.153	0.209	0.986	0.025	0.424	0.595	0.073
5B	29-Aug-11	6.3	0.783	2.479	0.000	0.385	0.154	0.212	1.051	0.018	0.425	0.868	0.060
7A	22-Feb-11	6.1	0.783	0.041	—	0.460	0.012	0.079	0.450	0.034	0.185	0.216	0.034
7A	24-Feb-11	5.8	0.783	6.921	—	0.439	0.039	0.080	0.377	0.005	0.140	0.268	0.127
7A	1-Mar-11	6.3	0.783	10.001	0.000	0.486	0.115	0.123	0.577	0.007	0.145	0.271	0.114
7A	8-Mar-11	6.4	0.783	0.291	—	0.567	0.019	0.116	0.502	0.013	0.160	0.154	0.093
7A	30-Mar-11	6.2	0.783	0.614	0.000	0.203	0.105	0.089	0.407	0.009	0.235	0.327	0.086
7A	21-Apr-11	6.1	0.783	0.882	0.000	0.944	0.038	0.107	0.308	0.026	0.265	0.370	0.074
7A	5-May-11	6.1	0.783	1.077	—	0.739	0.033	0.118	0.353	0.022	0.196	0.397	0.065
7A	19-May-11	6.2	0.783	1.271	—	0.745	0.032	0.120	0.372	0.030	0.180	0.443	0.058
7A	29-Jun-11	6.8	0.783	1.782	—	0.889	0.054	0.237	0.608	0.041	0.240	0.718	0.049
7A	29-Aug-11	6.4	0.783	2.537	—	1.095	0.113	0.265	0.626	0.053	0.327	0.873	0.038
7B	22-Feb-11	6.3	0.783	0.041	—	1.052	0.020	0.073	0.360	0.080	0.274	0.352	0.040
7B	24-Feb-11	6.1	0.783	0.110	—	0.243	0.040	0.083	0.728	0.010	0.110	0.793	0.069
7B	1-Mar-11	6.2	0.783	0.208	—	0.209	0.113	0.108	0.597	0.005	0.131	0.182	0.083
7B	8-Mar-11	6.4	0.783	0.273	0.000	0.743	0.020	0.118	0.609	0.037	0.219	0.412	0.100
7B	30-Mar-11	6.2	0.783	0.522	—	0.252	0.185	0.100	0.509	0.009	0.181	0.236	0.080
7B	21-Apr-11	6.2	0.783	0.865	0.000	0.576	0.057	0.109	0.534	0.017	0.241	0.385	0.079
7B	5-May-11	6.1	0.783	1.085	0.000	0.689	0.113	0.117	0.554	0.014	0.289	0.423	0.073
7B	19-May-11	6.1	0.783	1.245	0.000	0.549	0.036	0.114	0.577	0.018	0.192	0.417	0.065
7B	29-Jun-11	6.6	0.783	1.753	—	0.537	0.045	0.251	0.937	0.013	0.166	0.691	0.052
7B	29-Aug-11	6.4	0.783	2.423	—	0.809	0.109	0.219	0.986	0.026	0.364	0.798	0.042

[—] Empty cells indicate that geochemical data are unavailable

Table A.2 Dissolved concentrations of Mt. Pinatubo ash

Sample number	Sampling date	pH	A_{BET} (m^2/g)	Si (ppm)	Li (ppm)	Na (ppm)	K (ppm)	Mg (ppm)	Ca (ppm)	F (ppm)	Cl (ppm)	SO_4 (ppm)	PO_4 (ppm)
3A	21-Feb-11	3.2	0.698	0.001	–	0.649	0.425	0.093	2.293	0.045	36.470	4.361	0.099
3A	23-Feb-11	3.3	0.698	0.146	–	1.316	0.580	0.085	4.191	0.058	35.265	6.506	1.516
3A	1-Mar-11	3.2	0.698	8.464	0.000	0.403	0.359	0.188	4.627	0.068	35.316	5.579	2.454
3A	8-Mar-11	3.1	0.698	0.883	0.000	0.798	0.456	0.261	4.884	0.094	35.239	5.515	2.917
3A	30-Mar-11	3.2	0.698	2.126	0.001	0.143	0.130	0.542	5.308	0.114	35.315	5.783	2.972
3A	21-Apr-11	3.2	0.698	2.733	0.001	0.334	0.418	0.714	5.741	0.127	36.604	6.173	3.037
3A	5-May-11	3.2	0.698	3.193	0.001	0.357	0.415	0.780	5.598	0.127	35.515	5.851	3.332
3A	19-May-11	3.2	0.698	3.566	0.001	0.557	1.070	0.623	6.505	0.117	24.982	6.474	3.085
3A	29-Jun-11	3.2	0.698	5.001	0.001	0.327	0.494	1.807	6.881	0.140	38.297	7.772	3.210
3A	29-Aug-11	3.2	0.698	6.803	0.001	0.537	0.607	1.542	6.787	0.160	36.817	7.382	2.873
3B	21-Feb-11	3.2	0.698	0.002	–	0.317	0.180	0.092	2.302	0.019	35.011	4.555	0.115
3B	23-Feb-11	3.3	0.698	0.135	–	0.250	0.182	0.065	4.984	0.045	34.876	8.927	1.335
3B	1-Mar-11	3.1	0.698	0.534	0.000	0.195	0.219	0.162	5.440	0.071	37.060	9.647	2.370
3B	8-Mar-11	3.1	0.698	0.857	0.000	0.239	0.229	0.269	5.508	0.080	35.183	8.351	2.660
3B	30-Mar-11	3.1	0.698	2.144	0.000	0.203	0.152	0.529	6.458	0.102	36.278	8.736	3.255
3B	21-Apr-11	3.2	0.698	2.884	0.001	0.385	0.334	0.695	6.707	0.109	36.089	9.141	3.271
3B	5-May-11	3.2	0.698	3.442	0.001	0.290	0.256	0.797	6.565	0.105	35.379	8.904	3.295
3B	19-May-11	3.2	0.698	3.953	0.001	0.338	0.284	0.891	6.515	0.112	35.302	8.715	3.320
3B	29-Jun-11	3.2	0.698	5.426	0.001	0.424	0.437	1.714	7.595	0.143	39.850	10.855	3.254
3B	29-Aug-11	3.2	0.698	7.490	0.001	0.404	0.377	2.174	7.766	0.129	38.249	10.631	6.368
4A	21-Feb-11	4.1	0.698	0.007	–	0.627	0.312	0.231	5.819	0.041	4.298	4.045	0.041
4A	23-Feb-11	4.2	0.698	0.070	–	0.575	0.279	0.033	4.284	0.030	4.077	9.073	0.490
4A	1-Mar-11	4.1	0.698	9.723	–	0.439	0.302	0.040	4.810	0.038	4.040	8.642	1.131
4A	8-Mar-11	4.2	0.698	0.260	0.000	1.272	0.300	0.052	5.062	0.058	4.100	8.758	1.458
4A	30-Mar-11	4.3	0.698	0.553	0.000	0.123	0.099	0.053	5.552	0.064	4.152	8.809	1.944
4A	21-Apr-11	4.5	0.698	0.762	0.000	0.548	0.758	0.080	6.321	0.068	4.290	9.003	1.844
4A	5-May-11	4.5	0.698	0.862	0.000	0.509	0.752	0.089	6.386	0.071	4.281	9.110	1.894
4A	19-May-11	4.6	0.698	0.994	0.000	0.591	0.700	0.095	6.331	0.070	4.158	9.004	1.841

4A	29-Jun-11	4.7	0.698	1.529	0.000	0.744	0.520	0.168	6.538	0.055	3.669	10.412	2.027
4A	29-Aug-11	4.5	0.698	2.207	0.000	1.385	0.133	0.169	6.025	0.105	4.437	10.885	1.793
4B	21-Feb-11	4.1	0.698	0.024	–	2.287	0.340	0.043	2.509	0.086	4.311	4.257	0.049
4B	23-Feb-11	4.1	0.698	0.077	–	1.777	0.297	0.040	4.888	0.117	4.136	9.733	0.586
4B	1-Mar-11	4.1	0.698	0.191	–	0.152	0.180	0.051	4.942	0.047	3.784	8.865	1.196
4B	8-Mar-11	4.3	0.698	0.270	0.000	0.433	0.327	0.061	5.104	0.058	3.877	8.761	1.500
4B	30-Mar-11	4.4	0.698	0.597	0.000	0.138	0.160	0.065	5.586	0.068	4.038	9.028	1.917
4B	21-Apr-11	4.5	0.698	0.807	0.000	0.320	0.363	0.084	5.815	0.063	4.104	9.146	1.910
4B	5-May-11	4.5	0.698	0.966	0.000	0.341	0.373	0.116	5.869	0.076	4.104	9.158	1.875
4B	19-May-11	4.6	0.698	1.137	0.000	0.353	0.517	0.104	5.715	0.075	3.962	9.100	1.844
4B	29-Jun-11	4.7	0.698	1.573	0.000	0.242	0.405	0.190	6.401	0.085	4.372	11.612	1.779
4B	29-Aug-11	4.7	0.698	2.232	0.000	0.599	0.599	0.197	6.550	0.101	4.534	10.752	1.803
5A	21-Feb-11	5.2	0.698	0.052	–	0.526	0.013	0.020	1.541	0.025	0.432	3.050	0.013
5A	23-Feb-11	5.1	0.698	0.081	–	0.510	0.014	0.025	3.146	0.032	0.456	6.448	0.092
5A	1-Mar-11	5.1	0.698	12.094	–	0.302	0.084	0.127	3.785	0.039	0.486	6.767	0.160
5A	8-Mar-11	5.5	0.698	0.155	–	0.393	0.028	0.026	3.165	0.018	0.390	6.296	0.174
5A	30-Mar-11	5.5	0.698	0.227	0.000	0.091	0.064	0.016	3.247	0.023	0.377	6.786	0.160
5A	21-Apr-11	5.8	0.698	0.326	0.000	0.571	0.068	0.014	3.364	0.031	0.548	6.858	0.158
5A	5-May-11	6.0	0.698	0.390	0.000	0.688	0.039	0.015	3.509	0.037	0.459	7.221	0.159
5A	19-May-11	6.1	0.698	0.463	0.000	0.411	0.045	0.015	3.333	0.031	0.484	6.774	0.139
5A	29-Jun-11	5.9	0.698	0.647	0.000	0.369	0.131	0.040	2.551	0.030	0.690	7.967	0.134
5A	29-Aug-11	6.1	0.698	0.950	0.000	0.341	0.044	0.035	2.877	0.031	0.415	8.046	0.130
5B	21-Feb-11	5.2	0.698	0.037	–	0.794	0.017	0.137	1.609	0.048	0.458	2.729	0.015
5B	23-Feb-11	5.2	0.698	0.049	–	0.828	0.016	0.022	3.169	0.077	0.471	6.711	0.072
5B	1-Mar-11	5.2	0.698	0.135	–	0.168	0.081	0.053	3.239	0.013	0.345	6.363	0.131
5B	8-Mar-11	5.5	0.698	0.119	–	0.294	0.023	0.025	3.177	0.012	0.353	6.443	0.142
5B	30-Mar-11	5.5	0.698	0.232	0.000	0.086	0.050	0.014	3.144	0.020	0.330	6.578	0.127
5B	21-Apr-11	5.8	0.698	0.331	0.000	0.264	0.047	0.015	3.305	0.020	0.344	6.826	0.123
5B	5-May-11	5.9	0.698	0.404	0.000	0.287	0.086	0.016	3.269	0.026	0.422	6.781	0.122
5B	19-May-11	6.1	0.698	0.455	0.000	0.278	0.057	0.017	3.279	0.027	0.369	6.765	0.118
5B	29-Jun-11	5.9	0.698	0.639	0.000	0.189	0.082	0.020	2.781	0.028	0.341	8.352	0.114

5B	29-Aug-11	6.1	0.698	0.980	0.000	0.364	0.129	0.021	2.885	0.030	0.426	8.132	0.117
7A	21-Feb-11	6.1	0.698	0.070	–	0.360	0.008	0.158	5.603	0.016	0.045	3.263	0.005
7A	23-Feb-11	6.1	0.698	0.088	–	0.442	0.012	0.020	3.390	0.040	0.033	7.268	0.021
7A	1-Mar-11	7.6	0.698	14.457	–	0.327	0.062	0.059	4.361	0.014	0.061	7.224	0.035
7A	8-Mar-11	6.1	0.698	0.145	–	0.435	0.019	0.027	3.171	0.019	0.044	6.799	0.031
7A	30-Mar-11	5.8	0.698	0.186	0.000	0.071	0.049	0.014	3.067	0.001	–	6.999	0.029
7A	21-Apr-11	5.9	0.698	0.323	0.000	0.558	0.022	0.015	2.933	0.021	0.066	7.027	0.027
7A	5-May-11	6.1	0.698	0.381	0.000	0.622	0.029	0.021	3.500	0.023	0.059	7.156	0.027
7A	19-May-11	6.2	0.698	0.431	0.000	0.721	0.100	0.016	2.934	0.028	0.166	6.898	0.026
7A	29-Jun-11	6.1	0.698	0.586	0.000	0.504	0.025	0.045	1.951	0.025	–	8.197	0.025
7A	29-Aug-11	6.4	0.698	0.825	0.000	1.050	0.340	0.079	1.970	0.046	0.580	8.477	0.029
7B	21-Feb-11	5.9	0.698	0.072	–	0.759	0.020	0.035	1.969	0.049	0.122	3.718	0.008
7B	23-Feb-11	5.9	0.698	0.084	–	0.850	0.017	0.088	4.735	0.059	0.143	8.965	0.020
7B	1-Mar-11	5.7	0.698	0.237	–	0.118	0.045	0.023	3.988	0.011	0.015	8.629	0.022
7B	8-Mar-11	6.0	0.698	0.101	–	0.300	0.027	0.018	3.936	0.019	0.015	8.496	0.027
7B	30-Mar-11	5.9	0.698	0.177	0.000	0.089	0.045	0.015	3.944	0.034	0.016	8.664	0.024
7B	21-Apr-11	5.9	0.698	0.287	0.000	0.405	0.043	0.015	4.011	0.036	0.093	8.703	0.021
7B	5-May-11	6.1	0.698	0.388	0.000	0.430	0.035	0.039	4.144	0.074	0.243	9.134	0.021
7B	19-May-11	6.2	0.698	0.421	0.000	0.407	0.028	0.014	4.074	0.070	0.067	8.552	0.019
7B	29-Jun-11	6.0	0.698	0.573	0.000	0.330	0.032	0.035	3.127	0.080	0.093	10.564	0.018
7B	29-Aug-11	6.4	0.698	0.845	0.000	0.394	0.035	0.047	3.059	0.085	0.086	10.797	0.022

[—] Empty cells indicate that geochemical data are unavailable

Table A.3 Dissolved concentrations of Eyjafjallajökull ash

Sample number	Sampling date	pH	A_{BET} (m^2/g)	Si (ppm)	Li (ppm)	Na (ppm)	K (ppm)	Mg (ppm)	Ca (ppm)	F (ppm)	Cl (ppm)	SO_4 (ppm)	PO_4 (ppm)
3A	22-Feb-11	3.4	6.15	0.52	0.00	2.02	0.70	0.24	3.22	0.17	36.15	0.55	0.81
3A	24-Feb-11	3.5	6.15	3.97	0.00	1.67	0.56	0.26	6.18	0.21	35.44	0.50	1.01
3A	1-Mar-11	3.5	6.15	6.64	0.00	2.01	0.86	0.64	8.32	0.27	36.10	0.91	0.87
3A	8-Mar-11	3.6	6.15	4.75	0.00	2.78	0.81	0.48	8.19	0.28	35.77	0.70	0.61
3A	30-Mar-11	3.8	6.15	7.32	0.00	2.63	0.94	1.10	8.80	0.34	37.43	1.52	0.07
3A	21-Apr-11	3.9	6.15	9.26	0.00	2.62	1.20	1.21	9.70	0.33	35.98	1.66	0.0
3A	5-May-11	3.9	6.15	11.16	0.00	2.83	1.20	1.21	9.34	0.33	35.88	1.90	0.0
3A	19-May-11	4.0	6.15	6.77	0.00	2.81	1.15	1.23	9.43	0.32	35.71	2.04	0.0
3A	29-Jun-11	3.9	6.15	17.42	0.00	2.95	1.08	1.03	9.61	0.38	38.51	0.53	0.0
3A	29-Aug-11	4.1	6.15	20.57	0.00	3.00	1.05	1.07	9.72	0.36	37.01	3.20	0.0
3B	22-Feb-11	3.4	6.15	0.47	0.00	1.02	0.34	0.23	3.01	0.10	36.26	0.51	0.73
3B	24-Feb-11	3.5	6.15	1.74	0.00	1.34	0.37	0.36	5.71	0.17	35.15	0.43	0.82
3B	1-Mar-11	3.5	6.15	3.45	0.00	1.60	0.53	0.71	8.47	0.25	36.32	0.56	0.96
3B	8-Mar-11	3.8	6.15	4.49	0.00	1.77	0.57	0.69	7.91	0.26	35.37	0.67	0.79
3B	30-Mar-11	3.7	6.15	7.05	0.00	1.96	0.71	1.04	8.35	0.30	35.67	1.22	0.11
3B	21-Apr-11	3.8	6.15	9.38	0.00	2.09	0.74	1.13	8.60	0.29	36.21	1.56	0.05
3B	5-May-11	3.8	6.15	11.62	0.00	2.34	0.84	1.16	8.75	0.30	36.38	1.67	0.01
3B	19-May-11	3.9	6.15	13.60	0.00	2.48	0.89	1.18	8.74	0.30	37.13	1.86	0.0
3B	29-Jun-11	3.9	6.15	17.79	0.00	2.30	0.79	0.70	8.76	0.34	38.25	2.46	0.0
3B	29-Aug-11	4.0	6.15	23.79	0.00	2.51	0.82	1.17	9.05	0.33	36.91	2.62	0.0
4A	22-Feb-11	5.6	6.15	0.21	–	1.79	0.04	0.14	1.46	0.16	4.19	0.37	0.53
4A	24-Feb-11	6.5	6.15	4.74	0.00	1.23	0.11	0.18	1.85	0.10	3.44	0.41	0.51
4A	1-Mar-11	6.4	6.15	8.68	0.00	1.29	0.19	0.24	2.87	0.10	3.52	1.11	0.52
4A	8-Mar-11	7.2	6.15	1.65	0.00	1.42	0.05	0.24	2.86	0.10	3.32	0.41	0.37
4A	30-Mar-11	7.4	6.15	2.55	0.00	1.42	0.11	0.25	3.47	0.11	3.45	0.52	0.22
4A	21-Apr-11	7.4	6.15	3.61	0.00	1.80	0.07	0.28	3.65	0.12	3.45	0.64	0.20
4A	5-May-11	7.3	6.15	4.62	0.00	1.53	0.20	0.30	3.96	0.11	3.45	0.73	0.13
4A	19-May-11	7.1	6.15	5.69	0.00	2.01	0.07	0.31	4.33	0.13	3.42	0.77	0.11

4A	29-Jun-11	6.5	6.15	7.14	0.00	1.95	0.11	0.46	3.51	0.15	3.60	0.93	0.09
4A	29-Aug-11	6.9	6.15	2.56	0.00	2.15	0.13	0.50	3.40	0.18	3.57	1.28	0.21
4B	22-Feb-11	5.6	6.15	0.19	—	1.34	0.14	0.13	1.66	0.09	3.46	1.17	0.41
4B	24-Feb-11	6.3	6.15	0.76	0.00	1.05	0.12	0.18	2.10	0.09	3.33	0.72	0.39
4B	1-Mar-11	6.6	6.15	1.39	0.00	1.13	0.13	0.22	2.58	0.09	3.28	0.47	0.35
4B	8-Mar-11	7.1	6.15	1.67	0.00	1.30	0.07	0.25	3.00	0.10	3.20	0.52	0.30
4B	30-Mar-11	7.3	6.15	2.56	0.00	1.35	0.14	0.25	3.42	0.11	3.45	0.61	0.21
4B	21-Apr-11	7.4	6.15	3.61	0.00	1.57	0.15	0.30	4.00	0.12	3.73	0.70	0.17
4B	5-May-11	7.2	6.15	4.14	0.00	1.91	0.09	0.30	3.87	0.12	3.50	0.84	0.14
4B	19-May-11	7.1	6.15	4.63	0.00	1.75	0.23	0.32	4.19	0.10	3.68	0.96	0.12
4B	29-Jun-11	6.8	6.15	5.74	0.00	1.62	0.22	0.45	3.79	0.15	3.43	1.23	0.10
4B	29-Aug-11	7.1	6.15	7.21	0.00	1.77	0.21	0.49	3.96	0.14	3.53	1.50	0.08
5A	22-Feb-11	7.3	6.15	0.11	—	1.21	0.03	0.09	0.42	0.11	0.58	3.43	0.16
5A	24-Feb-11	8.3	6.15	10.74	—	1.03	0.07	0.13	1.21	0.06	0.43	4.17	0.16
5A	1-Mar-11	8.1	6.15	10.64	0.00	1.05	0.11	0.18	1.83	0.07	0.39	3.75	0.14
5A	8-Mar-11	8.5	6.15	1.83	0.00	1.28	0.04	0.20	2.29	0.08	0.40	4.06	0.11
5A	30-Mar-11	8.3	6.15	2.66	0.00	1.57	0.05	0.22	3.02	0.12	0.46	5.77	0.09
5A	21-Apr-11	7.7	6.15	3.43	0.00	1.68	0.08	0.25	3.41	0.12	0.46	7.38	0.09
5A	5-May-11	7.4	6.15	3.85	0.00	1.92	0.14	0.27	3.54	0.13	0.54	8.30	0.07
5A	19-May-11	7.2	6.15	4.27	0.00	2.34	0.79	0.31	3.88	0.11	1.75	9.12	0.06
5A	29-Jun-11	7.2	6.15	5.37	0.00	1.63	0.28	0.45	3.77	0.16	0.43	11.71	0.06
5A	29-Aug-11	7.5	6.15	6.72	0.00	2.02	0.17	0.47	3.64	0.19	0.63	13.85	0.07
5B	22-Feb-11	7.3	6.15	0.15	—	0.79	0.02	0.08	0.50	0.05	0.43	0.36	0.16
5B	24-Feb-11	8.4	6.15	0.78	—	1.12	0.11	0.25	1.88	0.06	0.47	0.59	0.15
5B	1-Mar-11	8.3	6.15	1.46	0.00	1.01	0.13	0.27	3.32	0.10	0.54	3.77	0.15
5B	8-Mar-11	8.5	6.15	1.75	0.00	1.14	0.05	0.20	2.09	0.08	0.40	0.34	0.13
5B	30-Mar-11	8.4	6.15	2.53	0.00	1.38	0.05	0.21	2.79	0.10	0.42	0.62	0.08
5B	21-Apr-11	7.7	6.15	3.30	0.00	1.49	0.12	0.24	3.31	0.10	0.46	0.70	0.09
5B	5-May-11	7.4	6.15	3.73	0.00	1.71	0.17	0.27	3.50	0.10	0.49	0.86	0.08
5B	19-May-11	7.2	6.15	4.12	0.00	1.49	0.24	0.28	3.58	0.11	0.50	0.74	0.07
5B	29-Jun-11	7.3	6.15	5.09	0.00	1.82	0.08	0.42	3.05	0.17	0.41	1.12	0.05

5B	29-Aug-11	7.5	6.15	6.42	0.00	1.70	0.30	0.43	3.52	0.16	0.46	1.09	0.07
7A	22-Feb-11	7.3	6.15	0.09	0.00	1.40	0.03	0.07	0.35	0.14	0.31	0.35	0.09
7A	24-Feb-11	8.4	6.15	10.52	—	1.03	0.06	0.13	1.21	0.07	0.09	0.49	0.08
7A	1-Mar-11	8.7	6.15	9.16	0.00	1.10	0.11	0.19	1.78	0.07	0.06	0.46	0.09
7A	8-Mar-11	8.7	6.15	1.96	0.00	1.25	0.04	0.21	2.21	0.08	0.09	0.54	0.05
7A	30-Mar-11	8.2	6.15	2.83	0.00	1.42	0.06	0.23	2.90	0.10	0.12	0.74	0.04
7A	21-Apr-11	7.6	6.15	3.61	0.00	1.74	0.07	0.26	3.34	0.12	0.11	0.68	0.06
7A	5-May-11	7.3	6.15	3.98	0.00	1.92	0.11	0.28	3.57	0.14	0.21	0.78	0.05
7A	19-May-11	7.1	6.15	4.42	0.00	1.90	0.10	0.30	3.81	0.14	0.20	0.94	0.05
7A	29-Jun-11	7.3	6.15	5.43	0.00	1.99	0.11	0.49	3.26	0.16	0.10	1.25	0.05
7A	29-Aug-11	7.3	6.15	6.89	0.00	2.10	0.17	0.50	3.78	0.20	0.27	1.44	0.06
7B	22-Feb-11	7.3	6.15	0.10	—	0.75	0.02	0.07	0.42	0.05	0.10	0.44	0.09
7B	24-Feb-11	8.7	6.15	0.86	—	0.96	0.06	0.23	2.62	0.09	0.14	2.61	0.10
7B	1-Mar-11	8.7	6.15	1.53	0.00	1.06	0.12	0.20	2.04	0.08	0.08	0.54	0.09
7B	8-Mar-11	8.7	6.15	1.94	0.00	1.13	0.05	0.23	2.17	0.08	0.08	0.57	0.07
7B	30-Mar-11	8.5	6.15	2.70	0.00	1.24	0.08	0.21	2.90	0.11	0.09	0.67	0.04
7B	21-Apr-11	7.6	6.15	3.43	0.00	1.64	0.16	0.28	3.48	0.13	0.28	0.98	0.07
7B	5-May-11	7.3	6.15	3.85	0.00	1.61	0.15	0.28	3.61	0.13	0.16	0.99	0.06
7B	19-May-11	7.2	6.15	4.22	0.00	1.60	0.15	0.29	3.75	0.12	0.15	0.95	0.05
7B	29-Jun-11	7.3	6.15	5.27	0.00	1.93	0.45	0.47	3.53	0.16	0.48	1.45	0.05
7B	29-Aug-11	7.4	6.15	6.60	0.00	1.76	0.27	0.50	3.79	0.18	0.17	1.51	0.07

[—] Empty cells indicate that geochemical data are unavailable

[0.0] Concentration was below limit of quantification and is presented as the lowest standard

Table A.4 Dissolved concentrations of Pacaya ash

Sample number	Sampling date	pH	A_{BET} (m^2/g)	Si (ppm)	Li (ppm)	Na (ppm)	K (ppm)	Mg (ppm)	Ca (ppm)	F (ppm)	Cl (ppm)	SO_4 (ppm)	PO_4 (ppm)
3A	22-Feb-11	3.3	0.143	0.020	—	0.189	0.108	0.028	0.466	0.009	36.471	0.682	0.0
3A	24-Feb-11	3.1	0.143	2.201	—	0.360	0.259	0.123	0.744	0.002	35.478	0.158	0.026
3A	1-Mar-11	3.1	0.143	4.394	—	0.308	0.221	0.210	0.792	0.003	35.234	—	0.039
3A	8-Mar-11	3.1	0.143	1.671	0.000	0.912	0.425	0.265	1.098	0.013	35.917	0.031	0.033
3A	30-Mar-11	3.2	0.143	3.787	—	0.292	0.063	0.317	1.300	0.011	36.377	0.120	0.186
3A	21-Apr-11	3.2	0.143	5.598	0.000	0.517	0.242	0.369	1.611	0.017	36.431	0.056	0.082
3A	5-May-11	3.3	0.143	6.982	0.000	0.674	0.357	0.408	1.792	0.017	36.441	0.029	0.036
3A	19-May-11	3.3	0.143	8.493	0.000	0.632	0.269	0.428	1.930	0.017	36.087	0.089	0.019
3A	29-Jun-11	3.4	0.143	12.084	0.000	0.703	0.301	0.902	2.957	0.028	39.502	—	0.007
3A	29-Aug-11	3.6	0.143	16.571	0.000	1.109	0.440	1.100	3.995	0.030	39.423	—	0.0
3B	22-Feb-11	3.2	0.143	0.053	—	1.185	0.429	0.030	0.280	0.103	37.575	0.070	0.0
3B	24-Feb-11	3.1	0.143	0.454	—	0.243	0.163	0.138	0.574	0.002	37.362	0.235	0.013
3B	1-Mar-11	3	0.143	0.969	—	0.162	0.085	0.179	0.705	0.002	35.766	0.060	0.023
3B	8-Mar-11	3.1	0.143	1.627	—	0.375	0.183	0.239	0.880	0.004	36.731	0.031	0.029
3B	30-Mar-11	3.1	0.143	3.689	0.000	0.296	0.065	0.288	1.152	0.012	37.217	0.059	0.0
3B	21-Apr-11	3.2	0.143	6.459	0.000	0.519	0.150	0.350	1.537	0.010	37.655	0.059	0.016
3B	5-May-11	3.2	0.143	8.123	0.000	0.569	0.177	0.378	1.703	0.008	37.685	0.064	0.015
3B	19-May-11	3.3	0.143	9.921	0.000	0.650	0.191	0.416	1.884	0.008	37.189	0.123	0.012
3B	29-Jun-11	3.4	0.143	14.308	0.000	0.781	0.241	0.930	2.953	0.015	41.218	0.013	0.011
3B	29-Aug-11	3.6	0.143	19.837	0.000	1.042	0.315	1.145	4.063	0.021	40.891	0.155	0.002
4A	22-Feb-11	4.3	0.143	0.011	—	0.586	0.239	0.045	0.271	0.028	3.218	0.146	0.001
4A	24-Feb-11	4.2	0.143	3.555	—	0.398	0.201	0.072	0.420	0.003	3.329	0.057	0.020
4A	1-Mar-11	4.1	0.143	6.692	—	0.464	0.208	0.123	0.562	0.003	3.312	0.047	0.026
4A	8-Mar-11	4.2	0.143	0.377	—	1.259	0.160	0.130	0.622	0.014	3.231	0.036	0.023
4A	30-Mar-11	4.4	0.143	0.782	—	0.081	0.025	0.117	0.519	0.006	3.592	—	0.014
4A	21-Apr-11	4.5	0.143	1.040	—	0.483	0.504	0.148	0.811	0.014	3.572	0.029	0.002
4A	5-May-11	4.5	0.143	1.196	—	0.671	0.481	0.133	0.685	0.009	3.758	0.018	0.0
4A	19-May-11	4.6	0.143	1.345	—	0.554	0.376	0.149	0.805	0.008	3.300	0.024	0.0

4A	29-Jun-11	4.5	0.143	1.660	—	0.456	0.432	0.259	1.269	0.007	3.706	—	0.0
4A	29-Aug-11	4.6	0.143	2.134	—	1.209	0.061	0.260	1.159	0.061	3.675	—	0.0
4B	22-Feb-11	4.3	0.143	0.024	—	1.947	0.222	0.059	0.281	0.101	3.394	0.012	0.001
4B	24-Feb-11	4.2	0.143	0.117	—	0.115	0.100	0.062	0.323	0.001	3.267	0.044	0.009
4B	1-Mar-11	4.1	0.143	0.275	—	0.134	0.122	0.107	0.511	0.002	3.202	0.120	0.015
4B	8-Mar-11	4.3	0.143	0.409	—	0.591	0.239	0.115	0.643	0.009	3.165	0.126	0.003
4B	30-Mar-11	4.4	0.143	0.803	—	0.072	0.016	0.136	0.543	0.007	3.313	0.036	0.0
4B	21-Apr-11	4.5	0.143	1.121	—	0.235	0.184	0.133	0.568	0.010	3.498	0.041	0.0
4B	5-May-11	4.5	0.143	1.274	—	0.293	0.229	0.146	0.608	0.006	3.535	0.027	0.0
4B	19-May-11	4.6	0.143	1.475	—	0.248	0.200	0.136	0.605	0.010	3.419	0.091	0.0
4B	29-Jun-11	4.6	0.143	1.789	—	0.251	0.196	0.236	1.003	0.013	3.538	—	0.0
4B	29-Aug-11	4.7	0.143	2.097	—	0.534	0.308	0.328	5.370	0.016	3.436	0.130	0.0
5A	22-Feb-11	5.7	0.143	0.020	—	0.488	0.015	0.055	0.424	0.016	0.381	0.122	0.002
5A	24-Feb-11	5.7	0.143	7.296	—	0.314	0.028	0.048	0.444	0.004	0.331	0.472	0.022
5A	1-Mar-11	5.9	0.143	10.095	—	0.157	0.047	0.088	0.436	0.002	0.318	0.081	0.006
5A	8-Mar-11	5.9	0.143	0.142	—	0.340	0.010	0.123	0.530	0.005	0.326	0.065	0.001
5A	30-Mar-11	6.1	0.143	0.198	—	0.036	0.019	0.130	0.583	0.003	0.310	—	0.0
5A	21-Apr-11	6.1	0.143	0.327	—	0.354	0.068	0.135	0.612	0.006	0.454	0.027	0.0
5A	5-May-11	6.1	0.143	0.381	—	0.239	0.026	0.138	0.640	0.008	0.361	0.019	0.0
5A	19-May-11	6.0	0.143	0.408	—	0.210	0.021	0.137	0.682	0.006	0.361	—	0.0
5A	29-Jun-11	5.8	0.143	0.526	—	0.296	0.060	0.207	0.872	0.003	0.416	—	0.0
5A	29-Aug-11	6.2	0.143	0.698	—	0.242	0.024	0.219	0.921	0.004	0.291	0.020	0.0
5B	22-Feb-11	5.4	0.143	0.015	—	0.969	0.020	0.033	0.213	0.054	0.591	0.098	0.002
5B	24-Feb-11	5.8	0.143	0.060	—	0.145	0.027	0.055	0.561	0.003	0.471	0.289	0.001
5B	1-Mar-11	5.8	0.143	0.124	—	0.068	0.032	0.092	0.591	0.001	0.438	—	0.000
5B	8-Mar-11	5.9	0.143	0.123	—	0.250	0.023	0.130	0.677	0.004	0.495	0.171	0.001
5B	30-Mar-11	6.1	0.143	0.214	—	0.044	0.024	0.122	0.638	0.004	0.484	0.015	0.0
5B	21-Apr-11	6.1	0.143	0.315	—	0.140	0.009	0.134	0.698	0.006	0.551	0.031	0.0
5B	5-May-11	6.1	0.143	0.366	—	0.225	0.050	0.143	0.733	0.005	0.523	0.022	0.0
5B	19-May-11	6.0	0.143	0.414	—	0.200	0.032	0.141	0.721	0.007	0.507	0.022	0.0
5B	29-Jun-11	5.8	0.143	0.524	—	0.156	0.021	0.217	1.060	0.005	0.526	0.012	0.0

5B	29-Aug-11	6.2	0.143	0.677	—	0.179	0.022	0.231	1.068	0.006	0.443	—	0.004
7A	22-Feb-11	6.1	0.143	0.026	—	0.491	0.046	0.068	0.386	0.018	0.176	0.260	0.005
7A	24-Feb-11	5.9	0.143	9.621	—	0.405	0.057	0.046	0.257	—	0.146	0.078	0.032
7A	1-Mar-11	6.6	0.143	10.923	—	0.129	0.050	0.066	0.570	0.003	0.006	0.362	0.007
7A	8-Mar-11	6.2	0.143	0.121	—	0.444	0.012	0.089	0.502	0.026	0.036	0.239	0.004
7A	30-Mar-11	6.3	0.143	0.178	—	0.064	0.036	0.111	0.514	0.008	0.064	0.139	0.001
7A	21-Apr-11	6.3	0.143	0.316	—	0.646	0.034	0.091	0.172	0.018	0.071	0.063	0.0
7A	5-May-11	6.1	0.143	0.355	—	0.647	0.037	0.092	0.160	0.014	0.067	0.021	0.0
7A	19-May-11	6.2	0.143	0.396	—	0.576	0.019	0.101	0.178	0.023	0.068	0.013	0.0
7A	29-Jun-11	6.1	0.143	0.498	—	0.581	0.031	0.135	0.062	0.021	—	—	0.0
7A	29-Aug-11	6.3	0.143	0.660	—	0.862	0.077	0.117	0.172	0.046	0.099	—	0.0
7B	22-Feb-11	6.2	0.143	0.015	—	0.871	0.016	0.041	0.242	0.093	0.303	0.074	0.001
7B	24-Feb-11	6.2	0.143	0.047	—	0.134	0.015	0.058	0.355	0.001	—	—	0.007
7B	1-Mar-11	6.3	0.143	0.104	—	0.077	0.048	0.076	0.563	0.002	0.010	0.106	0.002
7B	8-Mar-11	6.8	0.143	0.113	—	0.288	0.008	0.109	0.611	0.009	0.023	0.033	0.000
7B	30-Mar-11	6.4	0.143	0.210	—	0.043	0.029	0.130	0.638	0.008	0.025	—	0.0
7B	21-Apr-11	6.3	0.143	0.350	—	0.293	0.022	0.143	0.629	0.014	0.059	0.028	0.0
7B	5-May-11	6.2	0.143	0.410	—	0.331	0.026	0.141	0.623	0.011	0.125	0.035	0.001
7B	19-May-11	6.1	0.143	0.457	—	0.304	0.018	0.145	0.685	0.015	0.056	0.072	0.0
7B	29-Jun-11	6.0	0.143	0.613	—	0.300	0.016	0.188	0.955	0.011	—	—	0.002
7B	29-Aug-11	6.3	0.143	0.827	—	0.679	0.226	0.224	1.172	0.007	0.442	—	0.058

[—] Empty cells indicate that geochemical data was unable to be measured
[0.0] Concentration was below limit of quantification and is presented as the lowest standard

Table A.5 Dissolved concentrations of Tungurahua ash

Sample number	Sampling date	pH	A_{BET} (m^2/g)	Si (ppm)	Li (ppm)	Na (ppm)	K (ppm)	Mg (ppm)	Ca (ppm)	F (ppm)	Cl (ppm)	SO_4 (ppm)	PO_4 (ppm)
3A	8-Mar-11	3.0	0.247	0.085	—	—	—	—	—	—	—	—	0.371
3A	11-Mar-11	3.1	0.247	0.315	0.000	0.944	0.543	0.078	0.757	0.240	38.348	0.460	0.516
3A	15-Mar-11	3.0	0.247	0.622	0.000	1.009	0.572	0.140	0.872	0.262	39.460	0.407	0.575
3A	30-Mar-11	3.1	0.247	1.998	0.000	0.283	0.105	0.197	1.060	0.236	39.427	0.362	0.548
3A	21-Apr-11	3.1	0.247	2.317	0.000	0.548	0.333	0.205	1.322	0.228	38.808	0.427	0.586
3A	5-May-11	3.1	0.247	3.072	0.000	0.752	0.478	0.222	1.559	0.234	39.130	0.330	0.573
3A	19-May-11	3.2	0.247	4.307	0.000	0.633	0.240	0.219	1.711	0.221	38.490	0.323	0.606
3A	29-Jun-11	3.2	0.247	6.718	0.000	0.874	0.279	0.334	1.769	0.215	38.391	0.296	0.510
3A	29-Aug-11	3.2	0.247	11.090	0.000	0.681	0.259	0.356	1.655	0.242	40.768	0.358	0.371
3B	8-Mar-11	3.0	0.247	0.070	—	—	—	—	—	—	—	—	0.374
3B	11-Mar-11	3.1	0.247	0.267	0.000	0.260	0.169	0.068	0.677	0.215	39.321	0.427	0.498
3B	15-Mar-11	3.0	0.247	0.528	0.000	0.280	0.172	0.108	0.845	0.214	40.051	0.583	0.545
3B	30-Mar-11	3.1	0.247	1.922	0.000	0.254	0.069	0.198	0.991	0.202	38.591	0.357	0.566
3B	21-Apr-11	3.1	0.247	2.505	0.000	0.527	0.226	0.214	1.255	0.216	39.467	0.512	0.580
3B	5-May-11	3.1	0.247	3.341	0.000	0.525	0.218	0.217	1.436	0.216	38.227	0.442	0.590
3B	19-May-11	3.2	0.247	1.666	0.000	0.783	0.448	0.233	1.583	0.224	38.771	0.439	0.189
3B	29-Jun-11	3.2	0.247	7.283	–	0.831	0.460	0.333	1.536	0.253	40.245	0.413	0.552
3B	29-Aug-11	3.2	0.247	11.838	–	1.087	0.496	0.322	1.816	0.217	37.600	0.429	0.462
4A	8-Mar-11	4.1	0.247	0.048	—	—	—	—	—	—	—	—	0.097
4A	11-Mar-11	4.1	0.247	0.101	0.000	1.425	0.407	0.047	0.522	0.218	3.385	0.395	0.115
4A	15-Mar-11	4.2	0.247	0.202	—	1.599	0.321	0.048	0.490	0.217	3.563	0.414	0.118
4A	30-Mar-11	4.2	0.247	0.676	0.000	0.141	0.071	0.031	0.395	0.205	3.446	0.334	0.102
4A	21-Apr-11	4.3	0.247	0.794	0.000	1.360	0.512	0.069	0.751	0.224	3.489	0.315	0.067
4A	5-May-11	4.4	0.247	1.025	—	0.064	0.098	0.009	0.108	0.018	0.138	0.016	0.055
4A	19-May-11	4.3	0.247	1.243	0.000	1.528	0.362	0.061	0.713	0.211	3.451	0.312	0.052
4A	29-Jun-11	4.4	0.247	1.752	—	0.507	0.322	0.103	1.131	0.206	3.715	0.343	0.028
4A	29-Aug-11	4.6	0.247	2.229	—	0.702	0.438	0.063	0.791	0.205	3.752	0.380	0.010

4B	8-Mar-11	4.1	0.247	0.043	—	—	—	—	—	—	—	—	0.097
4B	11-Mar-11	4.1	0.247	0.099	0.000	0.420	0.284	0.033	0.370	0.205	3.691	0.454	0.129
4B	15-Mar-11	4.1	0.247	0.176		0.580	0.333	0.093	0.533	0.172	3.655	0.394	0.138
4B	30-Mar-11	4.2	0.247	0.688	0.000	0.136	0.058	0.034	0.390	0.190	3.551	0.248	0.104
4B	21-Apr-11	4.2	0.247	0.811	0.000	0.415	0.313	0.032	0.408	0.193	3.622	0.488	0.035
4B	5-May-11	4.3	0.247	1.056	0.000	0.606	0.413	0.035	0.437	0.188	3.743	0.395	0.053
4B	19-May-11	4.3	0.247	3.822	0.000	0.272	0.058	0.035	0.455	0.189	3.904	0.377	0.418
4B	29-Jun-11	4.4	0.247	1.815	—	1.444	0.311	0.094	1.025	0.244	3.842	0.261	0.006
4B	29-Aug-11	4.5	0.247	2.295	—	1.580	0.178	0.094	1.033	0.222	3.558	0.332	—
5A	8-Mar-11	5.2	0.247	0.040	—	—	—	—	—	—	—	—	0.039
5A	11-Mar-11	5.3	0.247	0.050	0.000	0.850	0.082	0.098	0.568	0.215	0.837	0.758	0.035
5A	15-Mar-11	5.3	0.247	0.068	0.000	0.756	0.028	0.045	0.375	0.200	0.735	0.309	0.050
5A	30-Mar-11	5.2	0.247	0.153	0.000	0.098	0.043	0.027	0.329	0.200	0.667	0.456	0.054
5A	21-Apr-11	5.1	0.247	0.183	0.000	0.377	0.100	0.043	0.476	0.203	0.710	0.508	0.050
5A	5-May-11	5.4	0.247	0.226	0.000	0.415	0.103	0.045	0.499	0.178	0.711	0.386	0.049
5A	19-May-11	5.5	0.247	0.265	0.000	0.516	0.090	0.043	0.483	0.207	0.751	0.357	0.049
5A	29-Jun-11	5.6	0.247	0.365	—	0.424	0.095	0.282	10.157	0.207	0.685	0.596	0.041
5A	29-Aug-11	5.6	0.247	0.483	—	0.409	0.063	0.077	0.742	0.185	0.632	0.416	0.032
5B	8-Mar-11	5.1	0.247	0.030	—	—	—	—	—	—	—	—	0.045
5B	11-Mar-11	5.2	0.247	0.041	0.000	0.455	0.083	0.045	0.433	0.201	0.805	0.416	0.060
5B	15-Mar-11	5.2	0.247	0.061	0.000	0.583	0.026	0.035	0.406	0.198	0.824	0.419	0.063
5B	30-Mar-11	5.2	0.247	0.179	0.000	0.139	0.076	0.029	0.336	0.218	0.800	0.437	0.061
5B	21-Apr-11	5.2	0.247	0.199	0.000	0.311	0.188	0.048	0.493	0.170	0.775	0.302	0.055
5B	5-May-11	5.3	0.247	0.253	—	0.435	0.209	0.069	0.561	0.174	0.822	0.657	0.054
5B	19-May-11	5.4	0.247	0.303	0.000	0.363	0.209	0.042	0.500	0.202	0.792	0.353	0.052
5B	29-Jun-11	5.5	0.247	0.429	—	0.471	0.158	0.062	0.680	0.193	0.838	0.312	0.045
5B	29-Aug-11	5.6	0.247	0.538	—	0.319	0.144	0.052	0.663	0.198	0.672	0.339	0.032
7A	8-Mar-11	5.5	0.247	0.044	—	—	—	—	—	—	—	—	0.022
7A	11-Mar-11	6.0	0.247	0.059	—	0.670	0.024	0.061	0.677	0.205	0.522	0.798	0.018
7A	15-Mar-11	5.7	0.247	0.073	0.000	0.615	0.018	0.048	0.395	0.197	0.428	0.387	0.034
7A	30-Mar-11	5.5	0.247	0.133	0.000	0.114	0.045	0.036	0.374	0.182	0.432	0.320	0.061

7A	21-Apr-11	5.4	0.247	0.177	0.000	0.826	0.040	0.055	0.193	0.210	0.565	0.328	0.054
7A	5-May-11	5.9	0.247	0.210	—	0.932	0.038	0.045	0.144	0.212	0.556	0.416	0.054
7A	19-May-11	6.0	0.247	0.235	0.000	0.932	0.035	0.047	0.123	0.188	0.521	0.449	0.051
7A	29-Jun-11	5.8	0.247	0.321	—	0.983	0.057	0.050	0.052	0.275	0.598	0.333	0.042
7A	29-Aug-11	5.7	0.247	0.431	—	4.588	0.215	0.023	0.074	0.419	3.426	—	0.030
7B	8-Mar-11	5.5	0.247	0.041	—	—	—	—	—	—	—	—	0.025
7B	11-Mar-11	5.6	0.247	0.053	0.000	0.479	0.022	0.043	0.434	0.192	0.540	0.407	0.036
7B	15-Mar-11	5.5	0.247	0.066	—	0.487	0.033	0.048	0.452	0.188	0.514	0.425	0.037
7B	30-Mar-11	5.4	0.247	0.138	0.000	0.102	0.041	0.032	0.373	0.193	0.458	0.247	0.043
7B	21-Apr-11	5.4	0.247	0.169	0.000	0.456	0.030	0.044	0.390	0.183	0.499	0.335	0.047
7B	5-May-11	5.5	0.247	0.201	0.000	0.596	0.091	0.046	0.387	0.182	0.599	0.472	0.046
7B	19-May-11	5.6	0.247	0.226	0.000	0.752	0.200	0.040	0.350	0.184	0.769	0.358	0.046
7B	29-Jun-11	5.7	0.247	0.311	—	0.535	0.060	0.079	0.470	0.184	0.549	0.385	0.040
7B	29-Aug-11	5.8	0.247	0.394	—	0.605	0.097	0.080	0.504	0.188	0.590	0.254	0.032

[—] Empty cells indicate that geochemical data are unavailable

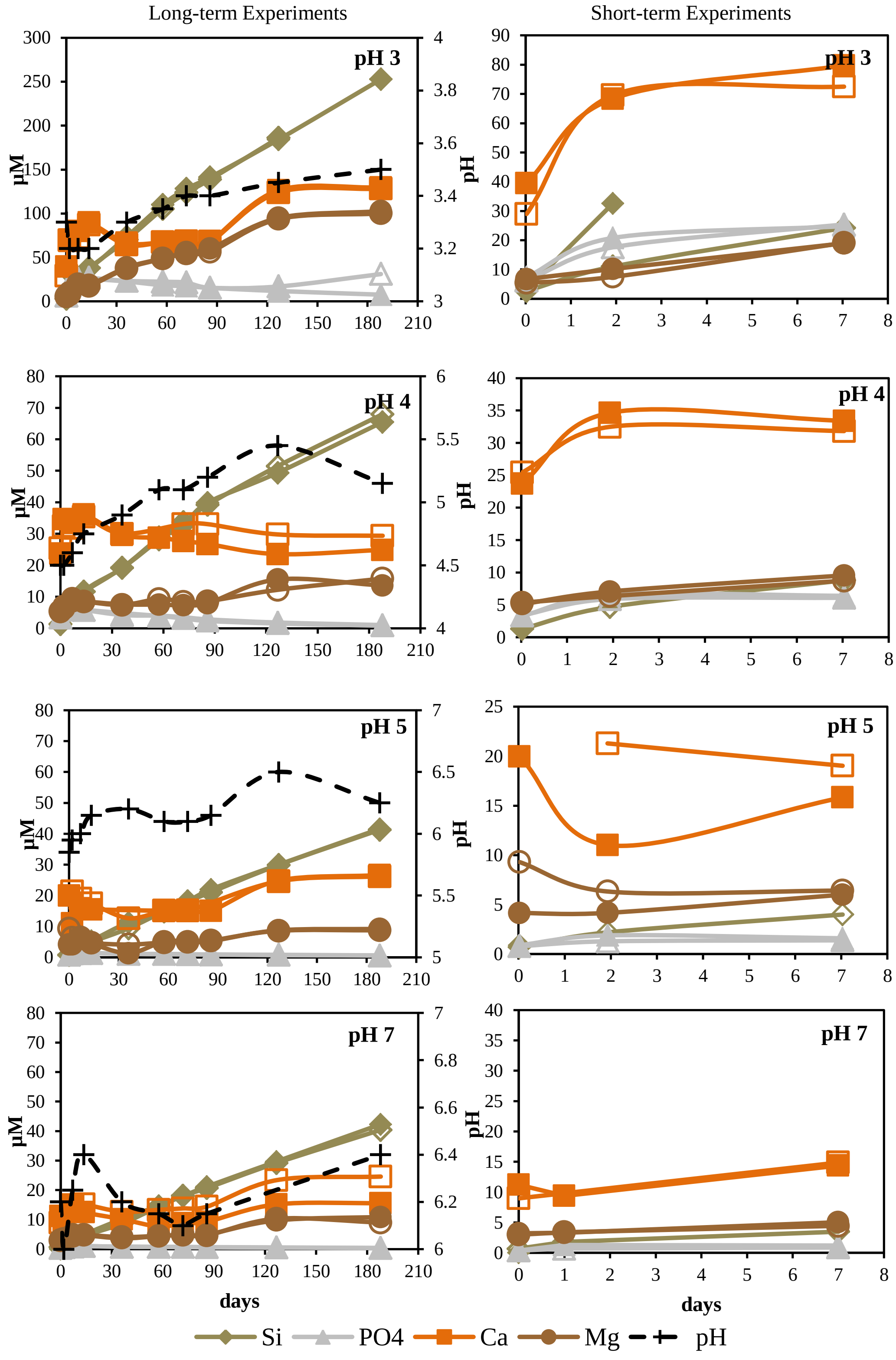

Fig. 1A. Mount St. Helens volcanic ash dissolution experiments. Concentrations of major ions (Si, PO_4, Ca, Mg) versus time in ~pH 3, 4, 5 and 7 solutions with associated replicates. Dashed line represents average pH at each sampling time point. Note different scales for each ash pH solution experiment.

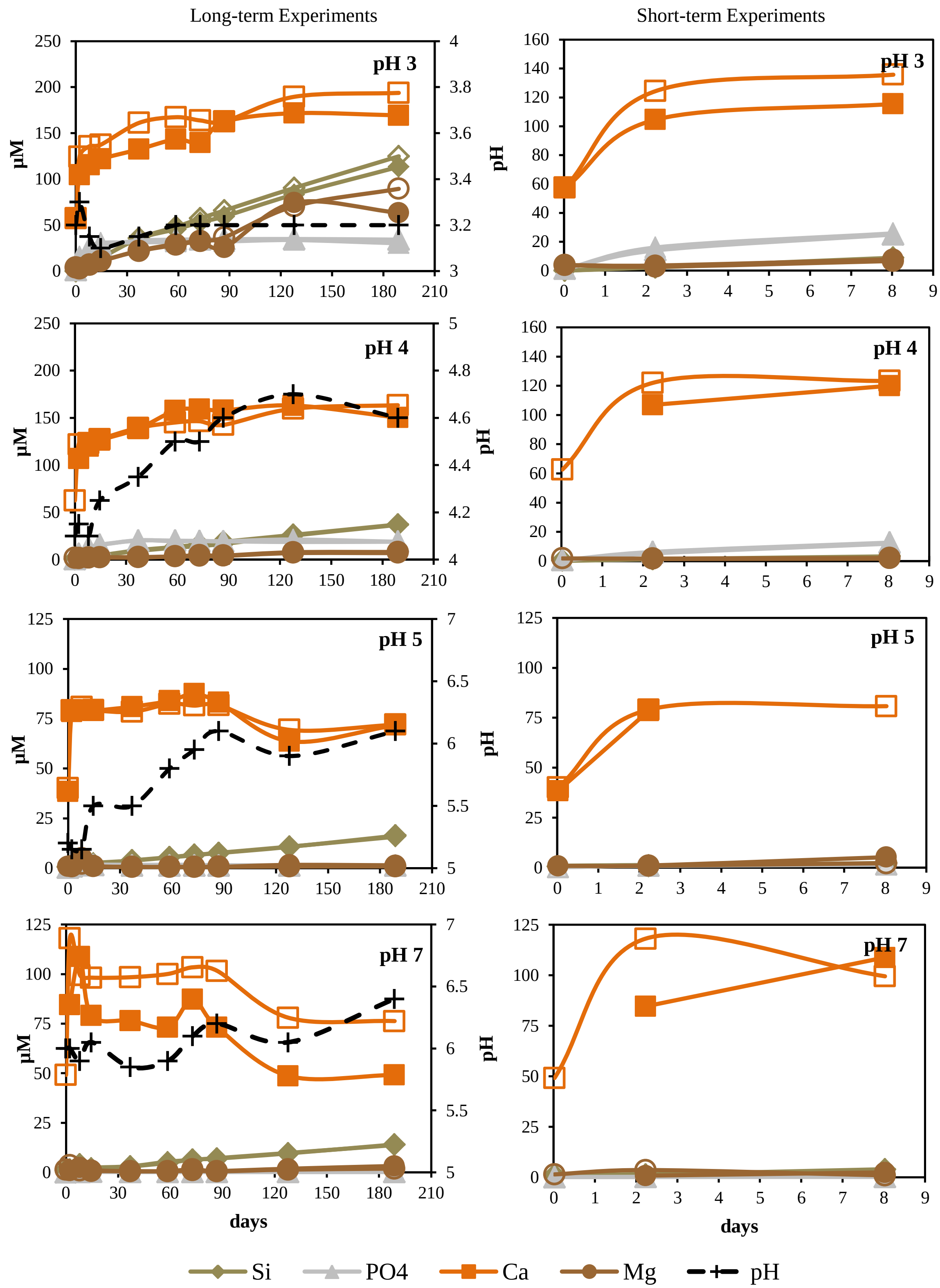

Fig. 2A. Pinatubo volcanic ash dissolution experiments. Concentrations of major ions (Si, PO_4, Ca, Mg) versus time in ~pH 3, 4, 5 and 7 solutions with associated replicates. Dashed line represents average pH at each sampling time point. Note different scales for each ash pH solution experiment.

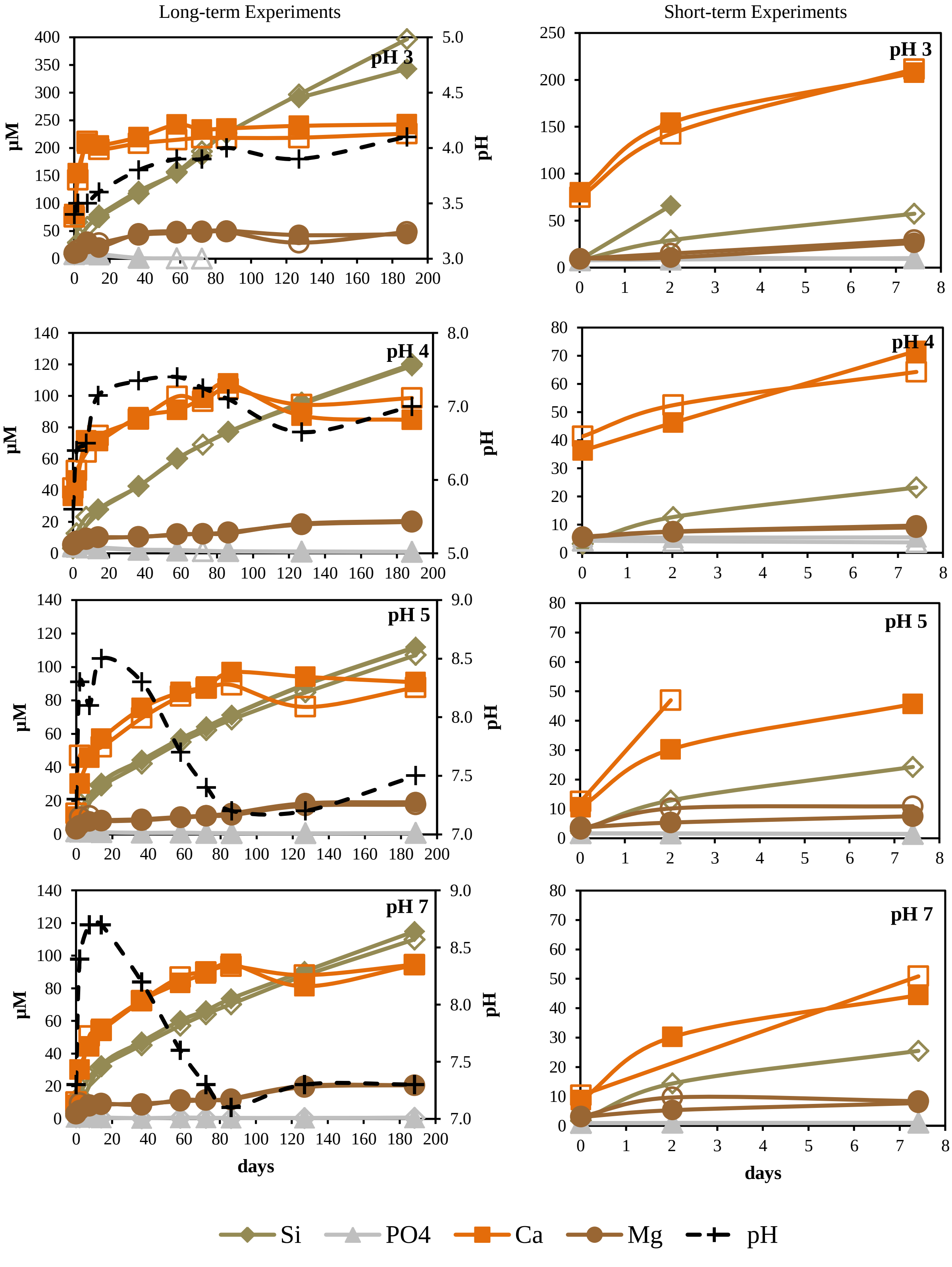

Fig. 3A. Eyjafjallajökull volcanic ash dissolution experiments. Concentrations of major ions (Si, PO_4, Ca, Mg) versus time in ~pH 3, 4, 5 and 7 solutions with associated replicates. Dashed line represents average pH at each sampling time point. Note different scales for each ash pH solution experiment.

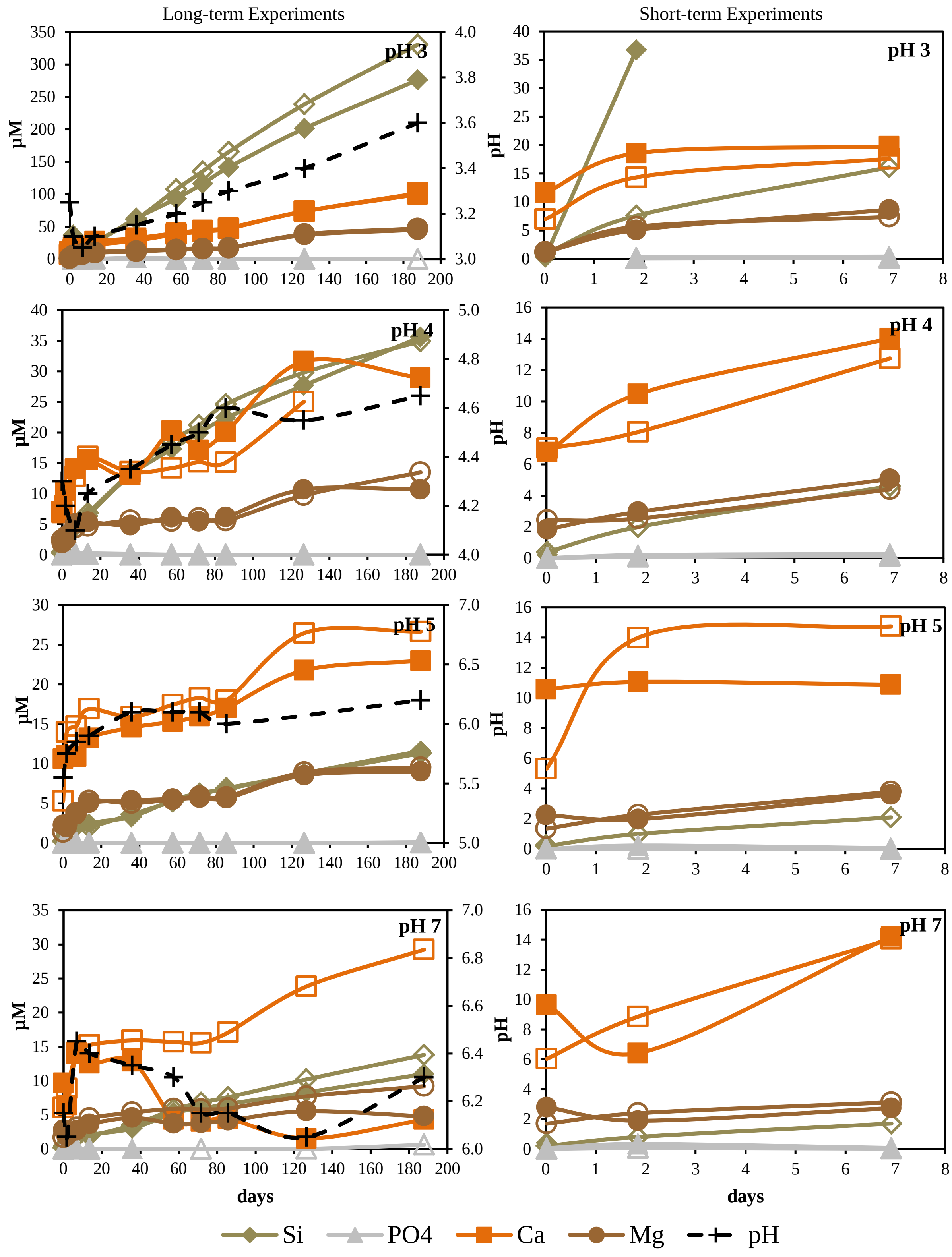

Fig. 4A. Pacaya volcanic ash dissolution experiments. Concentrations of major ions (Si, PO_4, Ca, Mg) versus time in ~pH 3, 4, 5 and 7 solutions with associated replicates. Dashed line represents average pH at each sampling time point. Note different scales for each ash pH solution experiment.

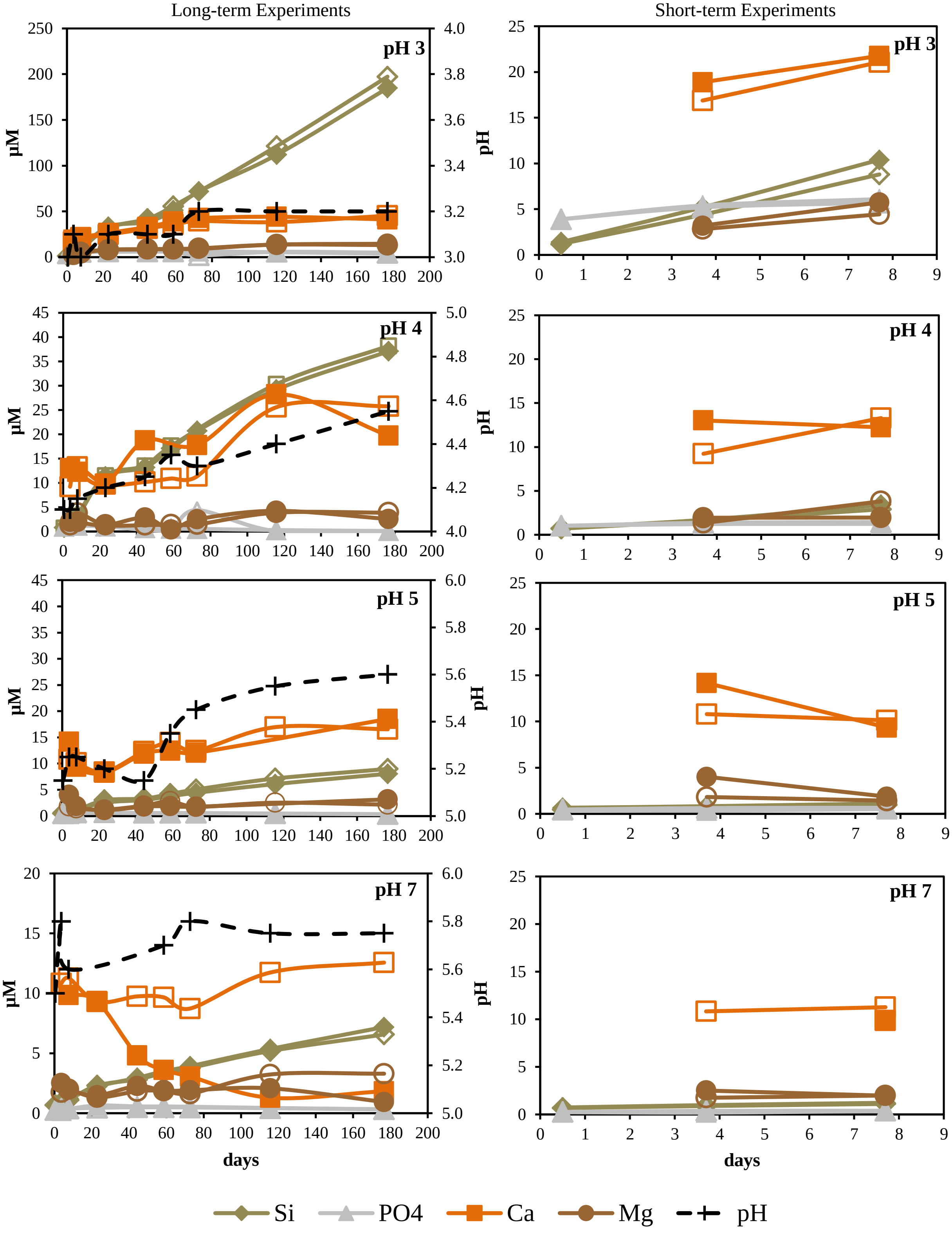

Fig. 5A. Tungurahua volcanic ash dissolution experiments. Concentrations of major ions (Si, PO_4, Ca, Mg) versus time in ~pH 3, 4, 5 and 7 solutions with associated replicates. Dashed line represents average pH at each sampling time point. Note different scales for each ash pH solution experiment.

Table 1B. Saturation indices of primary and secondary minerals in batch solution experiments
*, denotes 3rd sampling event of the experiment and its affiliated pH**s**
-, denotes no expected mineral phase

Experiment	*pH batch	pH	Quartz	*SiO_2 (a)	Clinoenstatite	Diopside	Ca-Olivine	Mg-Olivine	Anhydrite
			SiO2	SiO2	MgSiO3	CaMgSiO6	Ca2SiO4	Mg2SiO4	CaSO4
Mount St. Helens	3	*3.2	-0.53	-1.86	-14.7	-25.81	-38.6	-30.52	-4.9
Mount St. Helens	4	*4.6	-1.04	-2.37	-12.35	-21.19	-33.53	-25.32	-5.63
Pinatubo	3	*3.2	-0.91	-2.25	-15.57	-27.14	-39.26	-31.91	-3.76
Pinatubo	4	*4.1	-1.42	-2.76	-14.45	-24.24	-35.19	-29.13	-3.48
Eyjafjallajökull	3	*3.5	-0.18	-1.52	-13.57	-23.17	-36.06	-28.62	-4.41
Eyjafjallajökull	4	*6.4	-0.63	-1.97	-7.26	-10.71	-23.3	-15.55	-4.91
Pacaya	3	*3	-0.66	-1.99	-15.23	-27.16	-40.11	-31.45	-6.64
Pacaya	4	*4.2	-1.27	-2.6	-13.81	-24.17	-36.35	-28.01	-6.14
Mount St. Helens	3	3.5	–	-0.55	-12.12	-6.99	-35.51	–	-4.43
Mount St. Helens	4	5.1	-0.14	-1.14	-10.35	-17.59	-31.05	-22.19	-5.04
Mount St. Helens	5	6.2	-0.33	-1.33	-8.51	-13.72	-26.78	-18.31	-5.03
Mount St. Helens	7	6.4	-0.33	-1.33	-8.03	-13.06	-26.44	-17.36	-5.29
Pinatubo	3	3.2	–	-1.21	–	–	–	–	-3.72
Pinatubo	4	4.5	-0.41	-1.7	–	–	–	–	-3.54
Pinatubo	5	6.1	-0.78	-2.06	–	–	–	–	-3.66
Pinatubo	7	6.4	-0.81	-1.81	-11.35	-18.56	-30.35	-23.52	-5.96
Eyjafjallajökull	3	4.1	–	-0.73	–	–	–	–	-3.9
Eyjafjallajökull	4	6.9	-9.29	-1.18	–	–	–	–	-4.69
Eyjafjallajökull	5	7.5	–	-1.22	–	–	–	–	-4.64
Eyjafjallajökull	7	7.3	–	-1.21	–	–	–	–	-4.59
Pacaya	3	3.7	–	-0.51	-12.02	-20.87	-34.87	-26.17	–
Pacaya	4	4.6	-0.4	-1.4	-11.71	-20.16	-33.18	-24.66	–
Pacaya	5	6.2	-0.89	-1.89	-9.07	-14.89	-27.46	-18.88	-6.75
Pacaya	7	6.3	-0.91	-1.91	-9.16	-15.53	-28.53	-19.04	-7.79
Tungurahua	3	3.2	–	-0.69	-13.7	-24.1	-37.83	-29.34	-5.34
Tungurahua	4	4.6	-0.38	-1.38	-33.5	-20.9	-33.5	-25.88	-5.55
Tungurahua	5	5.6	-1.05	-2.05	-10.88	-18.16	-30.21	-22.35	-5.52
Tungurahua	7	5.8	-1.1	-2.1	-10.53	-18.46	-31.46	–	-6.62

Table 2B.(CONT of Table 1B) Saturated indices of primary and secondary minerals in batch solution experiments
*, denotes 3rd sampling event of the experiment and its affiliated pH**s**
-, denotes no expected mineral phase

Experiment	*pH batch	pH	Gypsum CaSO4:2H2O	Hydoxyapatite Ca5(PO4)3OH	Strengite FePO4:2H2O	Ferrihydrite Fe(OH)3	*Fe(OH)3 (a) Fe(OH)3	Goethite FeOOH
Mount St. Helens	3	*3.2	-4.62	-25.4	-1.38	-5.69	–	-1.52
Mount St. Helens	4	*4.6	-5.36	-18.03	0.88	-1.23	–	2.94
Pinatubo	3	*3.2	-3.47	-25.04	-1.44	-5.84	–	-1.74
Pinatubo	4	*4.1	-3.19	-17.71	1.24	-1.79	–	2.32
Eyjafjallajökull	3	*3.5	-4.12	-22.35	-1.47	-4.72	–	-0.62
Eyjafjallajökull	4	*6.4	-4.62	-1.51	0.26	1.08	–	5.19
Pacaya	3	*3	-6.36	-34.2	-2.97	-5.44	–	-1.26
Pacaya	4	*4.2	-5.87	-29.7	-1.35	-1.74	–	2.43
Mount St. Helens	3	3.5	-4.19	-25.3	0.54	-2.49	–	1.8
Mount St. Helens	4	5.1	-4.81	-20.33	-4.45	-4.93	–	-0.64
Mount St. Helens	5	6.2	-4.8	-12.96	-4.61	-3.83	–	0.47
Mount St. Helens	7	6.4	-5.05	-13.31	-4.81	-3.64	–	0.66
Pinatubo	3	3.2	-3.49	-28.99	–	–	-3.69	2.09
Pinatubo	4	4.5	-3.31	-20.63	–	–	-3.69	2.08
Pinatubo	5	6.1	-3.43	-12.87	–	–	-3.86	1.92
Pinatubo	7	6.4	-5.72	-22.15	-4.97	-3.66	–	0.63
Eyjafjallajökull	3	4.1	-3.67	–	–	–	-1.57	4.21
Eyjafjallajökull	4	6.9	-4.46	-9.25	–	–	-3.24	2.53
Eyjafjallajökull	5	7.5	-4.41	-6.38	–	–	-1.63	4.17
Eyjafjallajökull	7	7.3	-4.36	-7.32	–	–	-3.13	2.67
Pacaya	3	3.7	–	–	–	-2.14	–	2.15
Pacaya	4	4.6	–	–	–	-3.99	–	0.3
Pacaya	5	6.2	-6.51	-15.58	-5.38	-3.83	–	0.47
Pacaya	7	6.3	-7.55	-33.54	-10.39	-3.73	–	0.57
Tungurahua	3	3.2	-5.1	-30.72	-2.2	-5.24	–	-0.95
Tungurahua	4	4.6	-5.31	-26.9	-3.52	-3.65	–	0.65
Tungurahua	5	5.6	-5.29	-18.6	-4.83	-4.43	–	-0.13
Tungurahua	7	5.8	-6.38	-22.27	-2.71	-2.09	–	2.21